Hook length of the bacterial flagellum is controlled to nanometer-scale for optimal motility performance

Imke Spöring[2,*], Vincent A. Martinez[3,*], Christian Hotz[4,*], Jana Schwarz-Linek[3,*], Keara L. Grady[5], Josué M. Nava-Sedeño[6], Teun Vissers[3], Hanna M. Singer[7], Manfred Rohde[8], Carole Bourquin[4], Haralampos Hatzikirou[6,9], Wilson C. K. Poon[3], Yann S. Dufour[5], Marc Erhardt[1,2,7,$]

[1]Humboldt-Universität zu Berlin, Institute for Biology – Bacterial Physiology, Berlin, Germany

[2]Junior Research Group Infection Biology of *Salmonella*, Helmholtz Centre for Infection Research, Inhoffenstraße 7, 38124 Braunschweig, Germany

[3]School of Physics and Astronomy, The University of Edinburgh, Peter Guthrie Tait Road, Edinburgh, EH9 3FD, UK

[4]Department of Medicine/MED3, Chair of Pharmacology, University of Fribourg, Chemin du Musée 5, CH-1700 Fribourg, Switzerland

[5]Microbiology and Molecular Genetics, Michigan State University, 567 Wilson Road, East Lansing, MI 48824, USA

[6]Braunschweig Integrated Centre of Systems Biology (BRICS), Rebenring 56, D-38106 Braunschweig, Germany

[7]Department of Medicine/MED3, Microbiologie, University of Fribourg, Chemin du Musée 5, CH-1700 Fribourg, Switzerland

[8]Central Facility for Microscopy, Helmholtz Centre for Infection Research, Inhoffenstraße 7, 38124 Braunschweig, Germany

[9]Systems Immunology, Helmholtz Centre for Infection Research, Inhoffenstraße 7, 38124 Braunschweig, Germany

[*]Equal contribution

[$]Correspondence to: Marc Erhardt; Mailing address: Humboldt-Universität zu Berlin Institut für Biologie, Philippstr. 13, 10115 Berlin, Germany; Tel: +49 30 2093 49780; e-mail: marc.erhardt@hu-berlin.de

Abstract

Most bacteria swim in liquid environments by rotating one or several flagella. Each flagellum consists of a long external filament that is connected to a membrane-embedded basal-body by a short, curved structure: the hook. The length of the hook is controlled on a nanometer-scale by a sophisticated molecular ruler mechanism and it functions as a flexible universal joint allowing transmission of motor torque to the filament. However, why its length is stringently controlled has remained elusive. We engineered and studied a diverse set of hook length variants of *Salmonella enterica.* Measurements of plate-assay motility, single-cell swimming speed and directional persistence in quasi 2D and population-averaged swimming speed and body angular velocity in 3D revealed that the motility performance is optimal around the wild type hook length. We conclude that too short hooks may be too stiff to function as a junction and too long hooks may buckle and create instability in the flagellar bundle. Accordingly, peritrichously flagellated bacteria move most efficiently as the distance travelled per body rotation is maximal and body wobbling is minimized. Thus, our results suggest that the molecular ruler mechanism evolved to control flagellar hook growth to the optimal length consistent with efficient bundle formation. The hook length control mechanism is therefore a prime example of how bacteria evolved elegant, but robust mechanisms to maximize their fitness under specific environmental constraints.

Keywords: Flagellum, flagellar hook, nanometer-scale length control, motility performance, single cell tracking, differential dynamic microscopy, dark-field microscopy

Significance statement

Many bacteria use flagella for directed movement in liquid environments. The flexible hook connects the membrane-embedded basal-body of the flagellum to the long, external filament. Flagellar function relies on self-assembly processes that define or self-limit the lengths of major parts. The length of the hook is precisely controlled on a nanometer-scale by a molecular ruler mechanism. However, the physiological benefit of tight hook length control remains unclear. Here, we show that the molecular ruler mechanism evolved to control the optimal length of the flagellar hook, which is consistent with efficient motility performance. These results highlight the evolutionary forces that enable flagellated bacteria to optimize their fitness in diverse environments and might have important implications for the design of swimming micro-robots.

Introduction

Bacterial flagella are complex rotary nanomachines and enable directed movement of cells through various environments. The ability for locomotion and the presence of external flagellar structures contribute to pathogenesis and biofilm formation of many bacterial pathogens (1–4).

The bacterial flagellum is composed of three main structural parts: (i) a membrane-embedded basal body; (ii) a several micrometer long external filament; and (iii) the hook, a linking structure that connects the basal body and the rigid filament (5). The basal body complex functions as a motor to rotate the flagellum and includes a proton motive force (pmf) dependent flagellum-specific protein export machine (6, 7). Assembly of the flagellum initiates with formation of the export machinery within the cytoplasmic membrane, followed by formation of a rod structure that traverses the periplasmic space. Assembly of the hook starts upon completion of the P- and L-rings, which form a pore in the outer membrane and polymerize around the distal rod (8, 9). The extracellular, flexible hook structure functions as a universal joint and allows the conversion of the torque generated by the cytoplasmic motor into rotational motion of the flagellar filament irrespective of the cell body orientation (10). The self-assembly of the rod, hook and filament structures are controlled by different regulatory mechanisms. The length of the flagellar rod of ~25 nm is determined by the width of the periplasmic space (11), whereas the growth rate of flagellar filaments decreases with length and is controlled through pmf-dependent injection and diffusive movements of filament subunits inside the flagellar secretion channel (12). The length of the hook structure is controlled to ~55 nm through a molecular ruler mechanism (Fig. 1A) (13, 14). Upon termination of hook growth, the export apparatus switches secretion specificity from early ('rod/hook'-type) to late ('filament'-type) substrate secretion (15). This mechanism ensures that a functional hook-basal-body complex is present, on top of which the long flagellar filament made of several tens of thousands flagellin molecules can assemble (16). Control of hook length is lost in mutant strains defective of the *fliK* gene (17) and polymerization of hook subunits continues beyond the physiological length of 55 nm. This results in a wide, uncontrolled distribution of hook lengths, called polyhooks, and coincides with a failure of the export

106 apparatus to switch secretion specificity from early to late substrate secretion mode.
107 Thus, the FliK protein is responsible for both the measurement of hook length and the
108 transmission of the hook growth termination signal to the export apparatus, after which
109 the switch in substrate specificity occurs. Evidence has accumulated demonstrating that
110 FliK functions as a molecular ruler. FliK takes intermittent length measurements
111 throughout the assembly of the hook structure and terminates further hook growth when
112 the hook has reached a length of ~55 nm or longer (14, 18, 19).
113 Multiple flagella are randomly distributed over the cell surface in peritrichously flagellated
114 bacteria. The hook functions as a flexible linking structure that allows formation of flagellar
115 bundles at either cell pole irrespective of the relative position of the membrane-embedded
116 motors. When all flagella turn counterclockwise (CCW), they form a bundle rotating at
117 speed ω, causing the cell body to rotate in the opposite direction, and propel the cell
118 forward at speed v (run phase). Additionally, the body has a secondary motion
119 superimposed on the rotating axis called body wobbling, characterized by an angular
120 velocity Ω, due to the flagella bundle pushing the body off-axis (20, 21). When one or
121 more of the motors turn clockwise (CW), their associated flagella separate from the
122 bundle, causing a random change in the cell orientation (tumble). After all the motors have
123 reverted to CCW rotation, the flagellar bundle reforms and the bacterium swims in a new
124 direction. In homogenous environment (absence of gradient), the run-and-tumble
125 behavior results in an effective diffusive motion over large distances. Biasing the tumbling
126 rate allows chemotaxis, *i.e.* seeking attractants or escaping repellents in a chemo-
127 gradient (22–25). For flagellated bacteria swimming in a Newtonian liquid, *e.g.* buffer, v
128 is proportional to Ω and ω, which are determined by the geometry of both body and
129 flagellar bundle (26).
130 The relationship between hook length and motility is poorly studied. Loss of hook length
131 control diminishes motility (15); however, the mechanisms have not yet been examined.
132 The physiological benefit of tight hook length control remains unclear and was highlighted
133 recently as one of the big questions in bacterial hydrodynamics (27). We hypothesized
134 that the hook in its function as a universal joint might play a crucial role in the bundle state
135 and/or its stability. Thus, the need for proper hook length control would have evolved to

136 optimize motility in diverse environments. Here, we analyze the impact of variations in
137 hook length on the motility performance in semi-solid agar plate as well as liquid medium
138 in quasi 2D and 3D by single-cell tracking, differential dynamic microscopy (DDM) and
139 dark-field flicker microscopy (DFM). Our results reveal an optimal motility performance for
140 a wild type hook length of ~55 nm in respect to swimming speed, directional persistence
141 and propulsive efficiency. We conclude that the molecular ruler mechanism evolved to
142 control an optimal length of the hook structure for maximized motility performance via a
143 more stable bundle formation. Thus, a mechanism to control flagellar hook length
144 optimizes the cell's motility performance by minimizing random directional change during
145 the run phase.
146

147 ## Results and Discussion

148

149 **FliK molecular ruler deletion and insertion variants are secreted and functional**

150 The flagellar hook length is determined by secretion of a molecular ruler protein, FliK. We
151 engineered FliK mutants varying from 310 to 785 amino acids (aa) length using insertions
152 of α-helical parts of a homologous molecular ruler of the related virulence-associated type
153 III secretion system of *Yersinia*, YscP, or deletions of the central, α-helical domain of FliK
154 (Fig. 1B) (14, 18, 28). All FliK mutants were secreted and retained the ability to induce
155 the switch in secretion specificity to late substrate secretion as evidenced by comparable
156 levels of external flagellin FliC and induction of a Class 3 gene reporter (Fig. 1C,
157 Supplementary Fig. S1). The flagellation levels of the FliK mutants were not significantly
158 different with an average of 3.8 ± 1.5 flagella per cell (averaged across all FliK mutants)
159 compared to 3.6 ± 1.3 flagella per cell for the wild type (wt) (Fig. 1D, Supplementary Fig.
160 S2). We next purified hook basal body (HBB) complexes of the FliK length variation
161 mutants and determined the length of the hook structures by transmission electron
162 microscopy. FliK mutants ranging from 363 to 785 residues lengths retained a tight control
163 of hook length from 42 nm to 135 nm with a linear increase in hook length of 0.2 nm per
164 inserted amino acid (Fig. 1E, Supplementary Fig. S3). An increase of 0.2 nm per inserted

amino acid is consistent with an alpha-helical conformation of the ruler domain of FliK, as suggested before (18). The two shortest FliK mutants, $FliK_{310}$ and $FliK_{335}$, displayed partially uncontrolled hook lengths, indicating that a minimal FliK length is needed for effective hook length control (Fig. 1E, Supplementary Fig. S3).

Hook length mutants display a pronounced motility defect in semi-solid medium

We next analyzed the set of hook length variation mutants for their motility phenotype in semi-solid agar plates (Fig. 1F+G, Supplemental Fig. S4). The motility halo size was substantially decreased for mutants with shorter or longer hooks (FliK ≤ 363 aa and FliK ≥ 520 aa) and peaked at hook lengths around the wt length of 55 nm (FliK = 405 aa). The observed motility defect for long and short hook mutants was independent of the motility buffer and agar concentration, while prolonged incubation highlighted the motility differences (Supplementary Fig. S4+S5). These observations suggest that the hook length of the wt is in some way optimal (Fig. 1F+G). We note, however, that the motility phenotype in semi-solid agar plates is a complex combination of bacterial growth, motility and chemotactic behavior (29, 30). We found that bacterial growth rate was not impaired in the FliK mutants (Supplementary Fig. S5). Further, the presence of motility halos for all hook length mutants indicated functional chemotaxis. However, in order to decouple chemotaxis from motility and to reveal the effect of hook length on the swimming behavior, we next performed single-cell tracking experiments.

Single-cell tracking reveals that hook length mutants have lower swimming speed and shorter directional persistence

To identify which behavioral parameter explains the phenotype of hook length mutants in semi-solid medium, we characterized single-cell behavior in a quasi 2D environment as described before (31). In the absence of chemotactic signals, we observed the effect of hook length variation on the basal run-and-tumble behavior. We found that cells with longer hook lengths (>75 nm; FliK > 520 aa) have reduced average swimming speed and tumble more frequently (Fig. 2A+B, Supplementary Movie S1). Consequently, the directional persistence and the effective diffusion coefficient (32) of the mutants are

195 reduced (Fig. 2C+D). Therefore, longer hooks affect the cell's ability to explore their
196 environment. We propose that these observations are largely responsible for the motility
197 phenotypes that we observed in semi-solid agar plates.
198 We hypothesized that variations in the hook length increase instability during formation
199 of the flagellar bundle. Indeed, events in which filaments underwent polymorphic
200 transformations without filaments leaving the bundle (by contrast with a single tight
201 bundle), leading to small deflections in swimming direction, have been previously
202 observed and speculatively associated with motor reversal (33). To determine if the
203 apparent increase in tumble bias is the result of an increased rate of polymorphic changes
204 in the bundle, which are not associated with reversions of the flagellar motor rotation, we
205 characterized the behavior of same hook mutants in non-chemotactic, smooth-swimming
206 cells (Δ*cheY*). Mutants lacking CheY do not tumble and thus do not respond to chemical
207 gradients and do not efficiently navigate the agar gel matrix of semi-solid agar plates (29).
208 Accordingly, we assessed the motility behavior of smooth-swimming hook length mutants
209 using 2D single-cell tracking. In the Δ*cheY* genetic background (che$^-$), hook length
210 mutants still have reduced swimming speeds and smaller diffusion coefficients when
211 compared to the wt hook length (Fig. 2E+H). Cells with hooks longer than 75 nm have a
212 higher probability of changing direction suddenly; events, which we will refer to as
213 'pseudo-tumbles' (Fig. 2F). In non-chemotactic, smooth-swimming Δ*cheY* mutants, these
214 'pseudo-tumbles' cannot be caused by reversions of the flagellar motor. Finally, che$^-$ hook
215 length mutants displayed a reduced directional persistence (Fig. 2G), because of a
216 general increase in the probability of large changes in swimming direction
217 (Supplementary Fig. S6). These observations suggest that the poorer swimming
218 performance in hook-length mutants is likely to be primarily due to decreased stability of
219 the flagellar bundle.
220 To further analyze the dependence of 'pseudo-tumble' events on flagellar hook length
221 and to estimate a tumbling rate, we calculated the directional autocorrelation function and
222 mean square displacement (MSD) of selected non-chemotactic (Δ*cheY*), smooth-
223 swimming hook length mutant from the single-cell tracking experiments (Supplementary
224 Fig. S7, Supplementary Text 1). The autocorrelation function measures the persistence

225 of bacterial motion and the MSD represents the spatial exploratory potential of each cell.
226 The observed trajectories of non-chemotactic, hook length mutants with a 'pseudo-
227 tumble' phenotype were fitted to a simple run-and-tumble migration model
228 (Supplementary Text 2, Supplementary Fig. S8), taking into account the curvature of the
229 tracks due to hydrodynamic interactions of bacteria swimming in quasi 2D close to the
230 surface. The fit of the run-and-tumble model to the trajectories of the non-chemotactic,
231 hook length mutants suggest that the directional persistence decreases with increasing
232 hook length (Fig. 2G, Supplementary Fig. S7). We concluded that the pseudo tumble
233 events of the non-chemotactic mutants arise from a mechanical instability of the hook,
234 similar to the tumbling mechanism of *V. alginolyticus* (34).
235
236 **Non-chemotactic long hook mutants display a pseudo-tumble behavior**
237 The conclusion we have reached leads to an interesting prediction of the behavior of hook
238 mutants in agar gels. Chemotactic (che$^+$) bacteria can navigate through an agar gel matrix
239 due to their run-and-tumble motility behavior (Fig. 3A) (29). However, non-chemotactic,
240 smooth-swimming (Δ*cheY*) cells are trapped because tumbling is required to efficiently
241 escape the agar gel matrix (Fig. 3B). However, if the increased flagellar bundle instability
242 in hook mutants conferred on them a 'pseudo-tumble' phenotype, then we may expect
243 che$^-$ long hook mutants to regain the ability to migrate through an agar gel matrix. A
244 similar pseudotaxis behavior has previously been observed for non-chemotactic *E. coli*
245 mutants, where point mutations in the switch complex proteins FliG and FliM allowed
246 random motor rotational switching in the absence of chemotactic stimuli (29), as well as
247 in a non-chemotactic *A. tumefaciens* strain, where suppressor mutations in the hook, the
248 *fliK* gene and the motor force generators were isolated that allowed the che$^-$ cells to
249 navigate through semi-solid agar (35).
250 We analyzed the motility behavior of non-chemotactic, smooth-swimming hook length
251 mutants to test our prediction. The motility halo size of che$^+$ hook length mutants peaked
252 around the wt hook length (Fig. 1F, Fig. 3A). In contrast, che$^-$ long hook mutants
253 performed substantially better than che$^-$ mutants with shorter and wt hook length (Fig.
254 3B), in accordance with our suggestion that long hook lengths confer a pseudo-tumble

255 phenotype. We also noticed a big difference in the speed of spreading, che⁻ mutants
256 needed to be incubated ~5× longer to reach comparable halo sizes. This indicates that
257 pseudo-tumbling events occur less frequently than tumbling, *i.e.* due to motor reversal.
258 There is an interesting difference in appearance, che⁻ colonies form disks rather than
259 typical chemotactic rings confirming the pseudo-tumble events are not related to
260 chemotaxis and thus not associated with motor reversal.
261

262 **Motility parameters are optimal for wt hook length in 3D liquid environment**

263 All the experiments described so far pertain to bacteria swimming close to a hard surface
264 or in a gel matrix. In a final set of experiments, we measured swimming speed *v* and body
265 angular velocity Ω using high-throughput DDM and DFM in a 3D liquid environment (26,
266 36, 37). DDM and DFM experiments were performed with bacteria grown in TB medium
267 at 30 °C, which did not affect the overall motility behavior (Supplementary Fig. S9,
268 Supplementary Text 3). We recorded over 10^4 cells swimming in a 3D liquid medium (i.e.,
269 in bulk) for each of the hook length mutants. We found that the population-averaged
270 swimming speed *v* was maximal whereas the population-averaged body angular velocity
271 Ω was minimal over the range FliK ≥ 363 aa and FliK ≤ 480 aa, encompassing the wt
272 (FliK = 405 aa) (Fig. 4A+B, Supplementary Fig. S10A+B). Some variation in *v* and Ω were
273 observed between independent datasets, but this disappeared when we calculated the
274 population-averaged propulsive efficiency (processivity) $P = \frac{v}{\Omega}$, which is the average run
275 length per revolution. We found a clear maximum in processivity near the wt hook length,
276 in the range 363 aa ≤ FliK ≤ 405 aa (Fig. 4C, Supplementary Fig. S10C). Moreover, the
277 swimming speed distribution was narrower (the width of the speed distribution *S* is
278 minimal) in the range 363 aa ≤ FliK ≤ 570 aa (Supplementary Fig. S11), and swimming
279 trajectory appeared to be straighter (*R*, the ratio of two speeds measured at two length
280 scales, is minimal; see Methods for more details) in the range 405 aa ≤ FliK ≤ 520 aa.
281 Variations in $\frac{R}{R_{WT}}$ (with $\frac{R}{R_{WT}} > 1$) with FliK length are indicative of decreased directional
282 persistence in the cell trajectories (Fig. 4D, Supplementary Fig. S10D+E). The increase
283 in cell body angular velocity and the resulting decrease in processivity support the notion

that deviations from the wt hook length increase instability in the flagellar bundle and affect both swimming speed and directional persistence.

These experimental findings are independent of the tumbling behavior, as run-and-tumble strains displayed similar hook length dependency compared to the smooth-swimmers (Fig. 4, Supplementary Fig. S12). This was expected because the motility parameters are measured over a length-scale corresponding to the run length (<15 µm, distance between two tumble events). Differences are found in absolute values of *R* between run-and-tumble and smooth-swimmers at a given hook length due to tumbling events (Supplementary Fig. S10). However, the relative path straightness $\frac{R}{R_{WT}}$ scales for all hook mutants (Fig. 4, Supplementary Fig. S12).

Conclusion

In summary, our results provide substantial evidence that hook length control in peritrichously flagellated bacteria has been evolutionary selected to optimize the stability of the flagellar bundle and thus maximize swimming performance. We found that swimming speed and directional persistence of the trajectories of swimming bacteria are tightly related to the length of the hook structure. Recently, small polymorphic changes in the flagellar bundle have been observed without filaments leaving the bundle. These polymorphic changes create deflection in the swimming trajectory and have been associated speculatively with motor reversal (33). Our present work suggests these events might be associated with the run phase rather than motor reversal as they also occur in smooth swimming mutants. Thus, the role of hook length control may be to minimize such polymorphic changes by maximizing stability of the flagellar bundle during the run phase. We thus propose that the hook length control mechanism evolved to match the requirements for effective formation of the flagellar bundle. Stiffness is an inverse function of the hook length, *e.g.* stiffness increases with decreasing hook length. Too short hooks are too stiff to function as a universal joint whereas too long hooks may buckle and create too much instability, thus necessitating the need to control for an optimal length of the hook structure. Further, the observed higher processivity of hooks with wt length

313 appears to result in more efficient propulsion *i.e.* the cells are able to achieve higher
314 swimming speeds for the same energy expenditure. Our results are also consistent with
315 previous observations, where the wt hook of *E. coli* was modified to be twice more rigid
316 by binding of streptavidin and the flagellar bundle was unable to form (38). Hook length
317 control may also play a major role in other bacteria. Son and co-workers demonstrated
318 for the polar flagellated *Vibrio alginolyticus* that a buckling instability of the hook enables
319 the cell to 'flick' and re-orient (34). They suggested buckling occurs when the viscous
320 loads, *i.e.* force and torque exerted on the hook by the cell body and flagellum, exceed
321 the hook's buckling critical threshold. The associated critical torque and force are
322 inversely proportional to the hook length and its square, respectively. Thus, we expect
323 that changing the hook length of polar flagellated bacteria could dramatically alter the
324 instability region and enable more "flicking" events, which in turn would affect motility and
325 chemotactic behavior.
326 The function of the bacterial flagellum relies on the self-assembly of major components
327 with defined or self-limiting lengths (11, 12). Incomplete assembly or small deviations from
328 the blueprint result in a non-functional motility organelle with devastating consequences
329 for the organism. Thus, regulatory mechanisms evolved to determine the correct
330 dimensions of flagellar sub-assemblies and to ensure robust assembly of a functional
331 motility organelle. Our results demonstrate the selective advantage of a mechanism that
332 controls the length of the hook structure. In particular, our results suggest that the
333 molecular ruler mechanism evolved to determine the optimal length of the flagellar hook.
334 These results highlight the evolutionary forces that enable flagellated bacteria to optimize
335 their motility performance and fitness in diverse environments and might have important
336 implications for the future design of engineered, swimming micro-robots.

337 ## Materials and Methods:

338

339 **Bacterial strains, plasmids and media.** All bacterial strains used in this study are listed
340 in Supplementary Table S1. Cells were grown in either lysogeny broth (LB) (39) or TB
341 broth (1% Tryptone and 0.5% NaCl) at 30 °C or 37 °C. The generalized transducing phage
342 of *Salmonella enterica* serovar Typhimurium P22 *HT105/1 int-201* was used in all
343 transductional crosses (40). Insertions and deletions in the *fliK* gene were constructed
344 using λ-RED homologous recombination (41).

345

346 **Growth curve.** FliC-locked bacteria were grown overnight (o/n) at 37 °C and diluted to
347 OD_{600} of 0.001 in LB (final volume 200 μl) in a honeycomb multiwall plate. The bacteria
348 were incubated in the Bioscreen reader (EZExperiment software) at 37 °C with shaking
349 and OD_{600} was measured every 15 min and the measurements were blank corrected.

350

351 **Motility Assay.** Motility of the bacteria was assessed using soft agar plates containing a
352 range of agar concentrations from 0.2% – 0.35% essentially as described before (42).
353 Equal amounts of overnight cultures were inoculated into the soft agar plates using a pin
354 tool and incubated at 37 °C for 3 – 4 h (che^+) and 14 – 18 h (che^-), respectively. The
355 areas of the swimming halos (che^+) or disks (che^-) were analyzed using ImageJ and
356 normalized to the wt (hook length 55 nm; FliK = 405 aa).

357

358 **SDS-PAGE and Western blot.** FliC-phase locked bacteria were grown until late
359 exponential phase in LB. 2 ml of culture was used for harvesting cells (whole cell lysate)
360 and the supernatant by centrifugation (13,000 g, 4 °C, 5 min). Proteins were precipitated
361 using 10% TCA and the samples were resuspended in SDS sample buffer normalized to
362 their OD_{600}. Proteins were separated by SDS PAGE and Western blot was performed
363 using anti-FliK, anti-FliC and anti-DnaK antibodies.

364

365 **Hook-basal-body purification.** Purification of hook-basal body complexes without C-
366 ring was performed as described (43) with slight modifications. Briefly, bacteria were
367 grown in 500 ml culture until OD_{600} 1 – 1.5. Cells were harvested (8,000g, 4 °C, 10 min)
368 and resuspended in 30 ml ice-cold sucrose solution (0.5 M sucrose, 0.1 M Tris-HCl, pH
369 8). 3 ml lysozyme (10 mg/ml in sucrose solution) and 3 ml 0.1 M EDTA (pH 8) were added
370 to digest the peptidoglycan layer and to prepare the spheroplasts. The suspension was
371 stirred for 30 min on ice. 3 ml 10% Triton-X and 3 ml 0.1M MgSO4 were added to lyse
372 the spheroplasts. For complete lysis of the spheroplasts the mixture was stirred overnight
373 at 4 °C. Afterwards 3 ml 0.1M EDTA (pH 11) was added. Unlysed cells and cell debris
374 was pelleted by centrifugation (17,000 g, 4 °C, 20 min) and the pH was adjusted to pH 11
375 by adding 5 N NaOH. Following centrifugation (17,000g, 4 °C, 20 min) the flagella were
376 pelleted by ultracentrifugation (100,000 g, 4 °C, 1 h). The pellet was resuspended in 35
377 ml ice-cold pH 11 buffer (10% sucrose, 0.1 M KCl, 0.1% Triton-X) and centrifuged (17,000
378 g, 4 °C, 20 min) and the flagella were pelleted by ultracentrifugation (100,000 g, 4 °C, 1
379 h). The pellet was resuspended in 35 ml ice-cold TET-solution (10 mM Tris-HCl pH 8, 5
380 mM EDTA, 0.1% Triton-X) and the mixture again subjected to ultracentrifugation (100,000
381 g, 4 °C, 1 h). For depolymerization of the filaments, the flagella were resuspended in 35
382 ml pH 2.5 buffer (50 mM glycine, 0.1% Triton-X) and left at room temperature (RT) for 30
383 min. The debris was pelleted by centrifugation (17,000 g, 4 °C, 20 min) and the HBB were
384 collected by ultracentrifugation (100,000 g, 4 °C, 1 h). The pellet was air-dried and
385 resuspended in 200 μl TE solution (10 mM Tris-HCl pH 8, 5 mM EDTA). The samples
386 were stored at 4 °C and imaged the following day by negative staining electron
387 microscopy.
388
389 **Fluorescent microscopy.** FliC-phase locked bacteria were grown until mid-log phase in
390 LB or TB medium and immobilized on pre-coated 0.1% poly-L-lysine coverslips in a flow
391 cell as described (14). Cells were fixed with formaldehyde (2% final) and glutaraldehyde
392 (0.2% final). Flagella were stained using polyclonal FliC antibody (anti-rabbit) and anti-
393 rabbit coupled to Alexa Fluor 488. The membrane was stained using *N*-3-
394 Triethylammoniumpropyl-4-6-4-Diethylamino Phenyl Hexatrienyl Pyridinium Dibromide

395 (FM 4-64) and the DNA using 4′,6-diamidino-2-phenylindole (DAPI). Images were taken
396 using a Zeiss AxioObserver microscope at 100x magnification.
397
398 **Electron microscopy.** Hook samples were stored at 4 °C to straighten the hooks and
399 facilitate length measurements. The samples were negatively stained by 2% aqueous
400 uranyl acetate on a carbon film. Samples were imaged using a Zeiss TEM 910 at an
401 acceleration voltage of 80 kV with calibrated magnifications. Images were recorded using
402 a Slow-Scan CCD camera (ProScan, 1024x1024, Scheuring, Germany) with ITEM-
403 Software (Olympus Soft Imaging Solutions, Münster, Germany) software. Hook length
404 was measured using ImageJ.
405
406 **Luciferase assay.** The luciferase assay was performed as described before (19). The
407 plasmid pRG19 (*motA*::*luxCDABE*) was used for monitoring the switch from early
408 substrate secretion to late substrate secretion. The class 3 gene *motA* is expressed only
409 upon HBB completion. Synchronization of flagellar gene expression was achieved by
410 placing the AnTc inducible *tetA* promotor upstream of the *flhDC* gene (44). Cells were
411 grown in white clear-bottom 96-well plates (Greiner) and production of light and the OD_{600}
412 was measured over time using a Varioskan Flash multiplate reader (Thermo Fisher).
413 After blank correction, relative light units (RLU) were calculated as:

414 $$RLU = light \cdot \left(\frac{OD595\ t=0}{OD595\ t=n}\right).$$

415
416 **2D single-cell tracking and behavioral analysis.** Overnight cultures were incubated in
417 a shaking (200 rpm) incubator at 37 °C in LB broth. Overnight cultures were diluted 1:100
418 into fresh LB medium and incubated shaking at 200 rpm at 37 °C for 2.5 h. After cells
419 reached the mid-exponential growth phase (OD_{600} ~0.5) cultures were diluted 1:50 in
420 fresh LB medium and 7 μl of the dilution were placed on a microscope slide, covered with
421 a #1.5 22x22 mm coverslip, and sealed with VALAP (equal amount of petrolatum, lanolin,
422 and paraffin wax). The trajectories of swimming cells were recorded as previously
423 described (31). Briefly, cell positions were recorded using time-lapse phase contrast

424 microscopy (Nikon Eclipse TI-E with 10× Nikon CFI Plan Fluor, N.A. 0.30, W.D 16.0 mm)
425 at 10 frames per seconds (fps) (Zyla 4.2, Andor Technology Ltd.) for 100 seconds. The
426 field of view contained ~200 cells on average over 1.3 mm^2. Experiments were done in
427 triplicate with independent biological samples. Individual trajectories were reconstructed
428 as previously described using custom MATLAB (The MathWorks, Inc.) script
429 (https://github.com/dufourya/SwimTracker) (31) and u-track 2.1 (45). Tumbles were
430 detected using a two-state Markov-chain model representing the 'swimming' and
431 'tumbling' states with bi-variate Gaussian distributions of the relative acceleration and
432 angular acceleration. The Markov-chain model was trained on a reference dataset of wt
433 *S. enterica* cell trajectories. The diffusion coefficient of individual trajectories was
434 calculated using a covariance-based estimator (32) averaged over the time scales
435 exceeding the time scale of rotational diffusion (>10 s), over which cell trajectories are
436 diffusive. The directional persistence τ for each trajectory was calculated according to the
437 relationship $D = ½ v_0^2 \tau$, where D is the diffusion coefficient and v_0 is the average cell
438 speed.
439
440 **3D motility analyses using DDM and DFM.** For DDM/DFM experiments of bacterial
441 swimming behavior in 3D, cells are grown and washed, then loaded in sealed capillaries,
442 placed onto a microscope, and movies were recorded. Importantly, these five steps are
443 performed in parallel for a range of hook mutants, which allows precise measurement of
444 potential small difference in motility. Details are given below.
445 As standard protocols, overnight cultures were grown in LB for ~16 h using a shaking
446 incubator (200 rpm) at 30 °C. The overnight culture was diluted 1:100 in 35 ml TB and
447 grown for 2.5 – 3 h at 30 °C with shaking (200 rpm) to OD_{600} ~0.4 – 0.5. In some cases
448 (Fig. S9), overnight cultures were grown in LB for ~16 h using a shaking incubator
449 (200 rpm) at 37 °C. The overnight culture was diluted 1:100 in 35 ml LB and grown for
450 1.5 – 2 h at 37 °C with shaking (200 rpm) to OD_{600} ~0.4 – 0.5.
451 Cells were washed three times with motility buffer (MB, pH = 7.0, 6.2 mM K_2HPO_4, 3.8
452 mM KH_2PO_4, 67 mM NaCl, and 0.1 mM EDTA) by careful centrifugation to minimize
453 flagellar damage and were resuspended in MB to OD_{600} of 0.3. Washing step is performed

simultaneously for several samples and takes typically ~30 min for 6 samples.

Commercial glass capillaries (Vitrocom) with dimensions (L=5 cm x W=8 mm x H=400 μm, volume ~150 μl) were filled, sealed with petroleum jelly, and placed onto a fully-automated inverted microscope (Nikon TE300 Eclipse), and time-series of both phase-contrast (40 s long, Nikon Plan fluor 10× Ph1-NA=0.3 objective, Ph1 phase ring, 4.000 images at 512 × 152, 100 fps) and dark-field (10 s long, Nikon Plan Fluor 10× Ph1-NA=0.3 objective, Ph3 phase ring, 2.000 images at 512 × 152, 200 fps) movies are consecutively recorded continuously for ~1 h using an Hamamatsu ORCA-Flash 4.0 camera. One capillary at a time was prepared within 1 – 2 min, the movie was recorded immediately and then proceeded with next sample. Once all sample were prepared, continuous recording started. For 6 samples, this results in movie recorded every ~5 min for each capillary. Movies were recorded in bulk conditions (i.e. 100 μm above inner glass wall) to avoid interactions with wall.

From DDM analysis of the phase-contrast movies, the mean v and width σ (and consequently the relative width S = σ / v) of the swimming speed distribution $P(v)$, averaged over 10^4 cells, were extracted. Details can be found elsewhere (36, 37, 46) and only an overview is given below. Based on low-optical resolution, DDM characterizes the spatio-temporal fluctuations of the cell density via the so-called temporal autocorrelation function of the q-th Fourier component of the number density fluctuations, $f(q,\tau)$, with τ the delay time. q is the spatial frequency and defines a characteristic length-scale $L = 2\pi / q$. Given a suitable model for $f(q,\tau)$, kinetic parameters can be extracted. In case of swimming bacteria, DDM allows the measurement of an advective speed over a range of q values or length-scale L. The mean swimming speed v and width σ are extracted by averaging over the range $0.5 \leq q \leq 2$, corresponding to $3 \leq L \leq 13$ μm, and over the time window 10 min < t < 60 min.

A qualitative measure of the path straightness can also be estimated from DDM by calculating the ratio of speeds measured at two different length-scales, $R = v(L1) / v(L2)$, with e.g. $L1 < L2$. Theoretically, swimmers with a straight path yield $R = 1$. Deviations from straight-path, due to *e.g.* rotational diffusion or tumbling events, will increase this ratio above 1.

484 From DFM analysis of the dark-field movies, the body angular velocity Ω averaged over
485 ~10^4 cells in a few seconds was extracted. Details can be found elsewhere (26). Briefly,
486 the power spectrum of the flickering image of individual cells was Fourier transformed
487 and the lowest frequency peak in the average power spectrum was identified as $\Omega / 2\pi$.

Acknowledgments:

We thank Nadine Körner for expert technical assistance, Kelly T. Hughes for generous donation of strains and Howard Berg for discussions.

Funding information:

This work was supported in part by the Helmholtz Association Young Investigator grant VH-NG-932, the People Programme (Marie Curie Actions) of the Europeans Unions' Seventh Framework Programme grant 334030 (to M.E.), the intramural funding (Forschungsfond) of the University of Fribourg, Switzerland (to C.H. and M.E.), an EPSRC Programme Grant EP/J007404/1 (to V.A.M., J.S-L., W.C.K.P.); an ERC advanced grant AdG 340877 PHYSAPS (to V.A.M., J.S-L.,T.V., W.C.K.P.), a Marie Curie fellowship LivPaC, 623364 (to T.V.), and intramural funding from Michigan State University, USA (to Y.S.D., K.G.).

Author contributions:

Author contributions: I.S., V.A.M., C.H., J.S-L., J. M. N. S., H.H., W.C.K.P., Y.S.D. and M.E. designed research; I.S., V.A.M., C.H., J.S-L., J. M. N. S., K.G., H.M.S., M.R., H.H., Y.S.D. and M.E. performed research; I.S., V.A.M., C.H., J.S-L., J. M. N. S., T.V., H.H., W.C.K.P., Y.S.D. and M.E. analyzed data; M.R., C.H., H.H., W.C.K.P., Y.S.D. and M.E. contributed funding and reagents; I.S., V.A.M., J.S-L., J. M. N. S., H.H., Y.S.D. and M.E. wrote the paper with input from all authors.

509 **References:**

510 1. Josenhans C, Suerbaum S (2002) The role of motility as a virulence factor in bacteria. *Int J Med*
511 *Microbiol* 291:605–614.

512 2. Guttenplan SB, Kearns DB (2013) Regulation of flagellar motility during biofilm formation. *FEMS*
513 *Microbiol Rev* 37(6):849–871.

514 3. Erhardt M, Dersch P (2015) Regulatory principles governing *Salmonella* and *Yersinia* virulence.
515 *Front Microbiol* 6(949). doi:10.3389/fmicb.2015.00949.

516 4. Chaban B, Hughes HV, Beeby M (2015) The flagellum in bacterial pathogens: For motility and a
517 whole lot more. *Semin Cell Dev Biol* 46:91–103.

518 5. Chevance FFV, Hughes KT (2008) Coordinating assembly of a bacterial macromolecular machine.
519 *Nat Rev Microbiol* 6(6):455–65.

520 6. Paul K, Erhardt M, Hirano T, Blair DF, Hughes KT (2008) Energy source of flagellar type III secretion.
521 *Nature* 451(7177):489–492.

522 7. Minamino T, Namba K (2008) Distinct roles of the FliI ATPase and proton motive force in bacterial
523 flagellar protein export. *Nature* 451(7177):485–488.

524 8. Chevance FFV, et al. (2007) The mechanism of outer membrane penetration by the eubacterial
525 flagellum and implications for spirochete evolution. *Genes Dev* 21(18):2326–2335.

526 9. Cohen EJ, Hughes KT (2014) Rod-to-Hook Transition for Extracellular Flagellum Assembly Is
527 Catalyzed by the L-Ring-Dependent Rod Scaffold Removal. *J Bacteriol* 196(13):2387–2395.

528 10. Samatey FA, et al. (2004) Structure of the bacterial flagellar hook and implication for the molecular
529 universal joint mechanism. *Nature* 431(7012):1062–1068.

530 11. Cohen EJ, Ferreira JL, Ladinsky MS, Beeby M, Hughes KT (2017) Nanoscale-length control of the
531 flagellar driveshaft requires hitting the tethered outer membrane. *Science* 356(6334):197–200.

532 12. Renault TT, et al. (2017) Bacterial flagella grow through an injection-diffusion mechanism. *Elife*
533 6:e23136.

534 13. Hirano T, Yamaguchi S, Oosawa K, Aizawa S-I (1994) Roles of FliK and FlhB in Determination of
535 Flagellar Hook Length in *Salmonella typhimurium*. *J Bacteriol* 176(17):5439–5449.

536 14. Erhardt M, Singer HM, Wee DH, Keener JP, Hughes KT (2011) An infrequent molecular ruler
537 controls flagellar hook length in *Salmonella enterica*. *EMBO J* 30(14):2948–2961.

538 15. Williams AW, et al. (1996) Mutations in fliK and flhB Affecting Flagellar Hook and Filament Assembly
539 in *Salmonella typhimurium*. *J Bacteriol* 178(10):2960–2970.

540 16. Hughes KT, Gillen KL, Semon MJ, Karlinsey JE (1993) Sensing Structural Intermediates in Bacterial
541 Flagellar Assembly by Export of a Negative Regulator. *Science* 262(5137):1277–1280.

542 17. Patterson-Delafleld J, Martinez RJ (1973) A New *fla* Gene in Salmonella typhimurium -*flaR*- and Its
543 Mutant Phenotype-Superhooks. *Arch Mikrobiol* 90:107–120.

544 18. Shibata S, et al. (2007) FliK regulates flagellar hook length as an internal ruler. *Mol Microbiol*
545 64(5):1404–1415.

546 19. Erhardt M, et al. (2010) The role of the FliK molecular ruler in hook-length control in *Salmonella*
547 *enterica*. *Mol Microbiol* 75(5):1272–1284.

548 20. Darnton NC, Turner L, Rojevsky S, Berg HC (2007) On Torque and Tumbling in Swimming
549 *Escherichia coli*. *J Bacteriol* 189(5):1756–1764.

550 21. Hyon Y, Marcos, Powers TR, Stocker R, Fu HC (2012) The wiggling trajectories of bacteria. *J Fluid*
551 *Mech* 705:58–76.

552 22. Adler J (1966) Chemotaxis in Bacteria. *Science* 153(3737):708–716.

553 23. Macnab RM, Koshland DE (1972) The Gradient-Sensing Mechanism in Bacterial Chemotaxis. *Proc*
554 *Natl Acad Sci* 69(9):2509–2512.

555 24. Alon U, Surette MG, Barkai N, Leibler S (1999) Robustness in bacterial chemotaxis. *Nature*
556 397(6715):168–171.

557 25. Wadhams GH, Armitage JP (2004) Making sense of it all: bacterial chemotaxis. *Nat Rev Mol Cell*
558 *Biol* 5(12):1024–1037.

559 26. Martinez VA, et al. (2014) Flagellated bacterial motility in polymer solutions. *Proc Natl Acad Sci*
560 111(50):17771–17776.

561 27. Lauga E, Michelin S (2016) Stresslets induced by active swimmers. *Phys Rev Lett* 117(14):148001.

562 28. Wagner S, Stenta M, Metzger LC, Dal Peraro M, Cornelis GR (2010) Length control of the
563 injectisome needle requires only one molecule of Yop secretion protein P (YscP). *Proc Natl Acad*
564 *Sci* 107:13860–13865.

565 29. Wolfe AJ, Berg HC (1989) Migration of bacteria in semisolid agar. *Proc Natl Acad Sci* 86(18):6973–
566 6977.

567 30. Croze OA, Ferguson GP, Cates ME, Poon WCK (2011) Migration of Chemotactic Bacteria in Soft
568 Agar: Role of Gel Concentration. *Biophys J* 101(3):525–534.

569 31. Dufour YS, Gillet S, Frankel NW, Weibel DB, Emonet T (2016) Direct Correlation between Motile
570 Behavior and Protein Abundance in Single Cells. *PLoS Comput Biol* 12(9):e1005041.

571 32. Vestergaard CL, Blainey PC, Flyvbjerg H (2014) Optimal estimation of diffusion coefficients from
572 single-particle trajectories. *Phys Rev E - Stat Nonlinear Soft Matter Phys* 89(2):22726.

573 33. Turner L, Ping L, Neubauer M, Berg HC (2016) Visualizing Flagella while Tracking Bacteria. *Biophys*
574 *J* 111(3):630–639.

575 34. Son K, Guasto JS, Stocker R (2013) Bacteria can exploit a flagellar buckling instability to change
576 direction. *Nat Phys* 9:494–498.

577 35. Mohari B, et al. (2015) Novel Pseudotaxis Mechanisms Improve Migration of Straight-Swimming
578 Bacterial Mutants Through a Porous Environment. *MBio* 6(2):e00005-15.

579 36. Wilson LG, et al. (2011) Differential dynamic microscopy of bacterial motility. *Pysical Rev Lett*
580 106(1):18101.

581 37. Martinez VA, et al. (2012) Differential Dynamic Microscopy: A High-Throughput Method for
582 Characterizing the Motility of Microorganisms. *Biophys J* 103(8):1637–1647.

583 38. Brown MT, et al. (2012) Flagellar Hook Flexibility Is Essential for Bundle Formation in Swimming

584 *Escherichia coli* Cells. *J Bacteriol* 194(13):3495–3501.

585 39. Bertani G (2004) Lysogeny at Mid-Twentieth Century: P1, P2, and Other Experimental Systems. *J*
586 *Bacteriol* 186(3):595–600.

587 40. Sanderson KE, Roth JR (1988) Linkage map of *Salmonella typhimurium*, edition VII. *Microbiol Rev*
588 52(4):485–532.

589 41. Datsenko KA, Wanner BL (2000) One-step inactivation of chromosomal genes in *Escherichia coli*
590 K-12 using PCR products. *Proc Natl Acad Sci* 97(12):6640–6645.

591 42. Gillen KL, Hughes KT (1991) Negative Regulatory Loci Coupling Flagellin Synthesis to Flagellar
592 Assembly in *Salmonella typhimurium*. *J Bacteriol* 173(7):2301–2310.

593 43. Aizawa S-I, Dean GE, Jones CJ, Macnab RM, Yamaguchi S (1985) Purification and characterization
594 of the flagellar hook-basal body complex of *Salmonella typhimurium*. *J Bacteriol* 161(3):836–849.

595 44. Karlinsey JE, et al. (2000) Completion of the hook-basal body complex of the *Salmonella*
596 *typhimurium* flagellum is coupled to FlgM secretion and *fliC* transcription. *Mol Microbiol* 37(5):1220–
597 1231.

598 45. Jaqaman K, et al. (2008) Robust single particle tracking in live cell time-lapse sequences. *Nat*
599 *Methods* 5(8):695–702.

600 46. Schwarz-Linek J, et al. (2016) *Escherichia coli* as a model active colloid: A practical introduction.
601 *Colloids Surfaces B Biointerfaces* 137:2–16.

602 47. Elgeti J, Benjaminkaupp U, Gompper G (2010) Hydrodynamics of Sperm Cells near Surfaces.
603 *Biophys J* 99(4):1018–1026.

604

605

606 ## Figure legends

607

608 **Fig. 1: Characterization of hook length variants and motility performance in semi-**
609 **solid media.** (A) Model of the flagellar hook length control mechanism. The yellow star
610 indicates the switch in substrate specificity within the export apparatus. (B) Engineered
611 FliK length variants. (C) Cellular (cell) and secreted (supernatant) levels of FliK and
612 flagellin (FliC). Loading control (DnaK). A representative gel of two independent
613 experiments is shown. (D) Flagellation of hook length variation mutants (mean number of
614 flagella per cell + s.d.). FliK mutants with uncontrolled hook length are highlighted in red.
615 Representative fluorescent microscopy images are shown in Fig. S2. (E) Correlation
616 between the length of the FliK molecular ruler and the hook length of FliK mutants with
617 controlled hook length (mean hook length ± s.d.; mean hook lengths of the uncontrolled
618 FliK mutants (red)). Representative electron micrographs are shown in Fig. S3. (F)
619 Quantification of swimming motility phenotype in plates containing 0.3% agar (mean
620 motility (black bars) normalized to the wt). Individual replicates are shown. (G)
621 Representative motility plate of data shown in panel F (FliK length in amino acids is
622 indicated; non-flagellated control strain Δ*fliHIJ* (–)).

623

624 **Fig. 2: Single-cell motility performance of hook length variants in quasi 2D.**
625 Distributions of single-cell motility parameters for different hook-length mutants in a WT
626 background (che^+). Distributions of (A) the average swimming speed of individual cells,
627 (B) tumble bias (where tumbles are detected as a sudden change in direction regardless
628 of the direction of the motor rotation), (C) directional persistence, (D) diffusion coefficient.
629 (E-H) Same distributions from the smooth swimming hook-length mutants due to deletion
630 of *cheY* (che^-). Each distribution was calculated from the behavior of more than 600
631 individual cells pooled from three independent experiments. Mean: +, median: ◊.
632 Uncontrolled hook length mutants are shown in red.

633

634 **Fig. 3: Motility behavior of chemotactic and non-chemotactic hook length variants**
635 **in semi-solid agar.** (A) Motility performance of chemotactic (che^+) and (B) non-

636 chemotactic (Δ*cheY*, che$^-$) hook length mutants in semi-solid agar plates with varying
637 agar concentrations (0.2%, 0.25%, 0.3%, 0.35% agar). The che$^+$ mutants were incubated
638 for 3-4 h whereas the che$^-$ mutants were incubated for 14-18 h, depending on the agar
639 concentration. For all panels, a representative motility plate is shown on the right-hand
640 side. FliK length in amino acids is indicated; (–) annotates the non-flagellated control
641 strain Δ*fliHIJ*. Individual replicates are shown and black bars represent the mean motility
642 normalized to the wt. FliK mutants with uncontrolled hook length are highlighted in red.
643
644 **Fig. 4: Motility performance of hook length mutants in 3D.** (A) Swimming speed v, (B)
645 body rotational speed Ω, (C) processivity $P=v/\Omega$, (D) straightness of trajectory R. Data
646 points represent individual experiments normalized to the wt (black bars; mean).
647 Uncontrolled hook length mutants are shown in red. All parameters were obtained by
648 normalizing the time-dependent parameters to the wt (FliK405) and by averaging over the
649 time-window 10 min<t<60 min.

650 # Figures

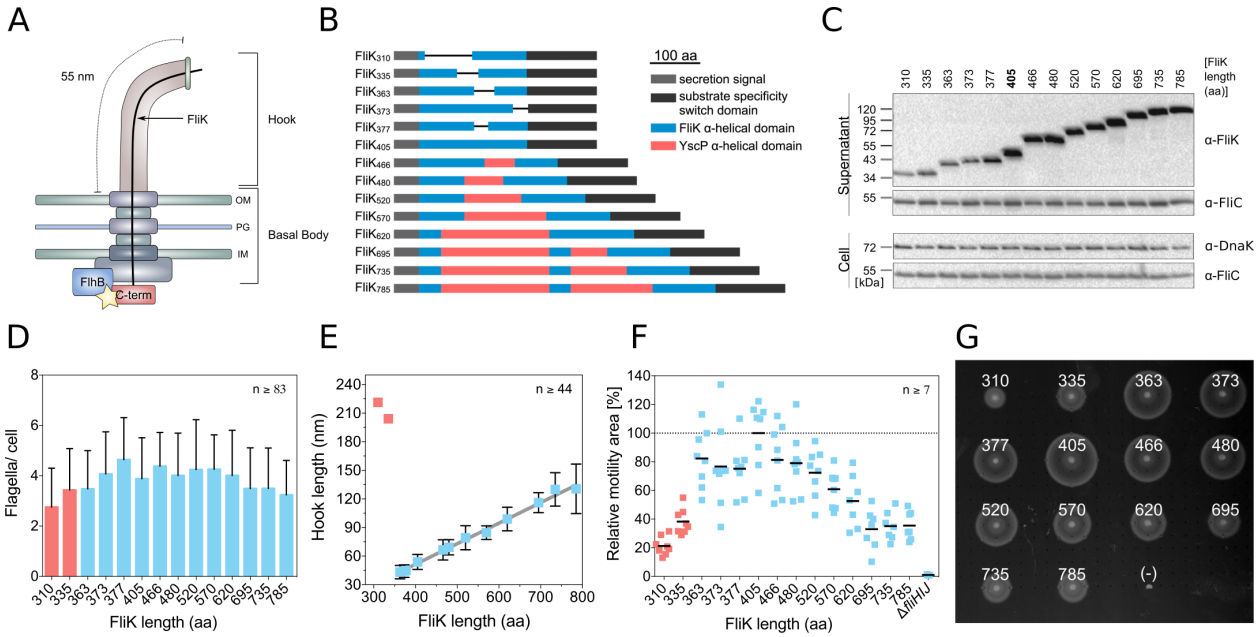

651

652 **Fig. 1: Characterization of hook length variants and motility performance in semi-**
653 **solid media.** (A) Model of the flagellar hook length control mechanism. The yellow star
654 indicates the switch in substrate specificity within the export apparatus. (B) Engineered
655 FliK length variants. (C) Cellular (cell) and secreted (supernatant) levels of FliK and
656 flagellin (FliC). Loading control (DnaK). A representative gel of two independent
657 experiments is shown. (D) Flagellation of hook length variation mutants (mean number of
658 flagella per cell + s.d.). FliK mutants with uncontrolled hook length are highlighted in red.
659 Representative fluorescent microscopy images are shown in Fig. S2. (E) Correlation
660 between the length of the FliK molecular ruler and the hook length of FliK mutants with
661 controlled hook length (mean hook length ± s.d.; mean hook lengths of the uncontrolled
662 FliK mutants (red)). Representative electron micrographs are shown in Fig. S3. (F)
663 Quantification of swimming motility phenotype in plates containing 0.3% agar (mean
664 motility (black bars) normalized to the wt). Individual replicates are shown. (G)
665 Representative motility plate of data shown in panel F (FliK length in amino acids is
666 indicated; non-flagellated control strain Δ*fliHIJ* (–)).

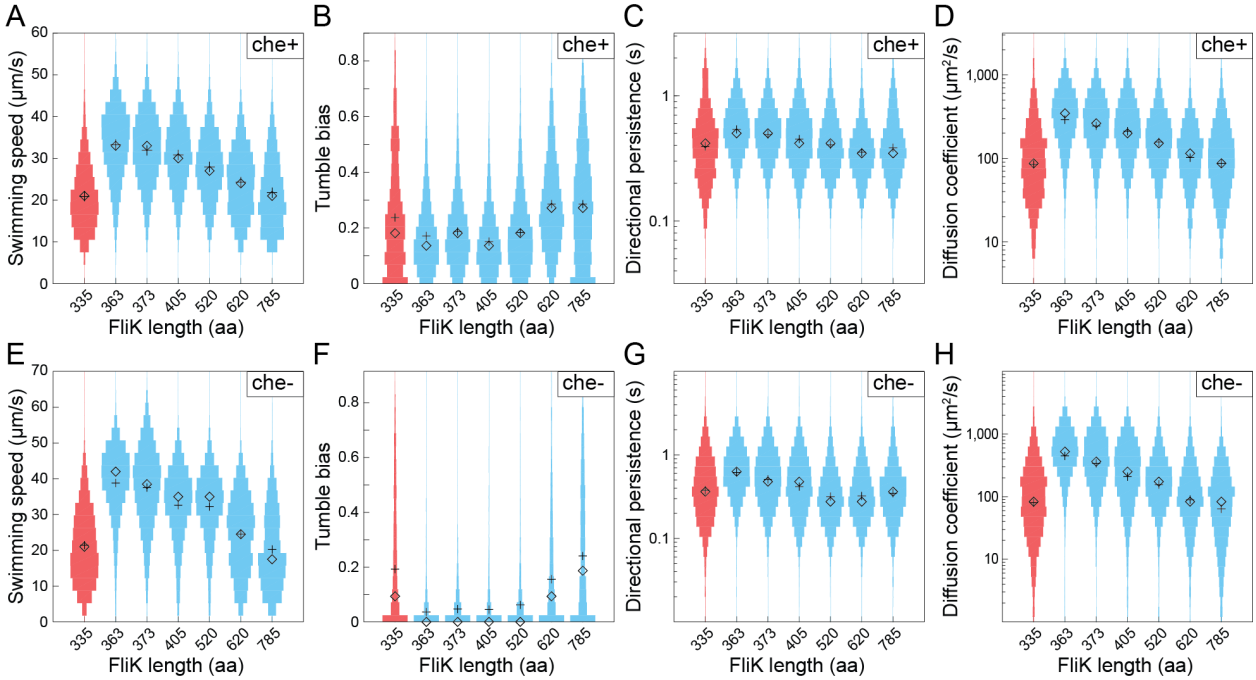

Fig. 2: Single-cell motility performance of hook length variants in quasi 2D. Distributions of single-cell motility parameters for different hook-length mutants in a WT background (che$^+$). Distributions of (A) the average swimming speed of individual cells, (B) tumble bias (where tumbles are detected as a sudden change in direction regardless of the direction of the motor rotation), (C) directional persistence, (D) diffusion coefficient. (E-H) Same distributions from the smooth swimming hook-length mutants due to deletion of *cheY* (che$^-$). Each distribution was calculated from the behavior of more than 600 individual cells pooled from three independent experiments. Mean: +, median: ◊. Uncontrolled hook length mutants are shown in red.

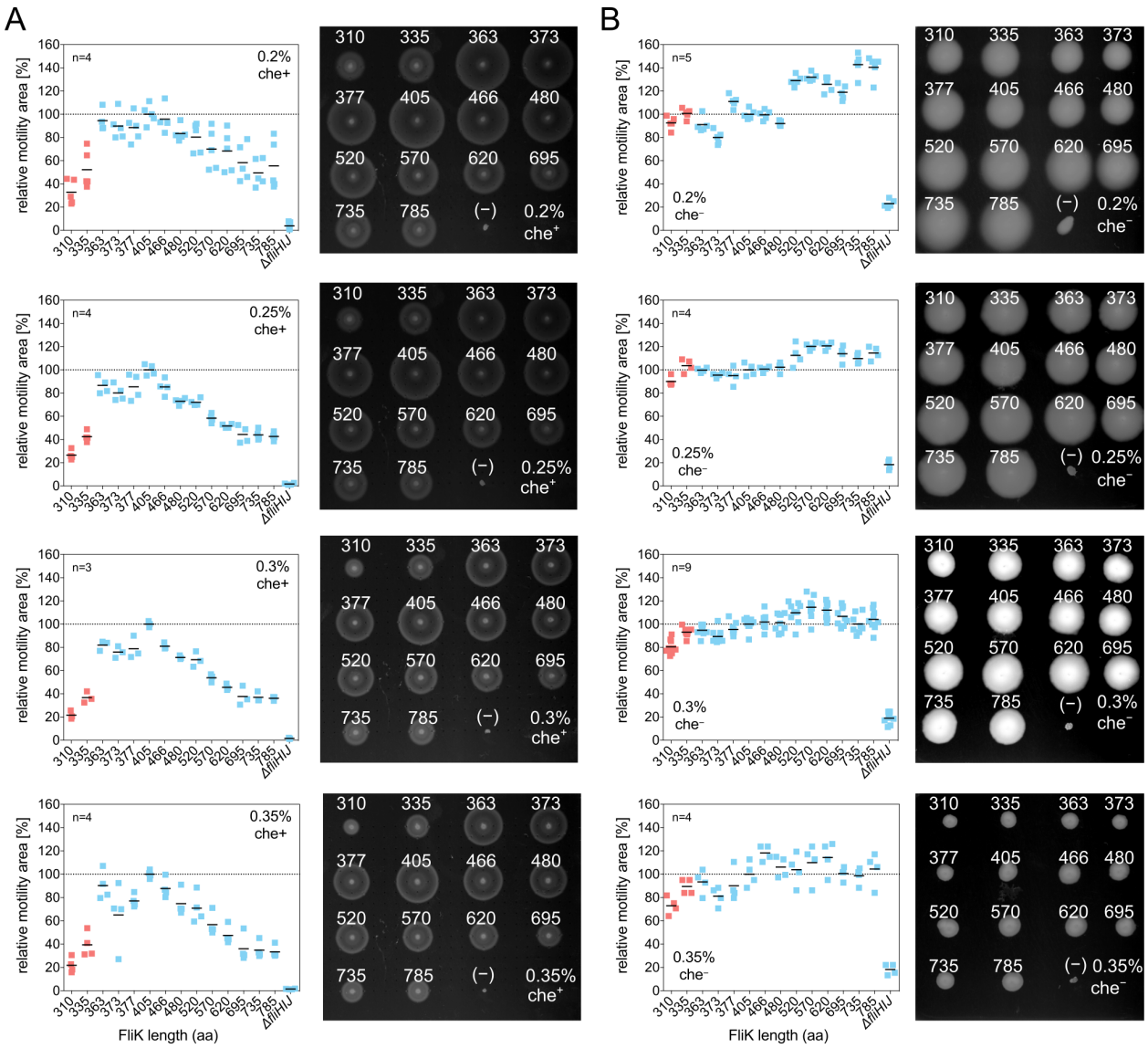

Fig. 3: Motility behavior of chemotactic and non-chemotactic hook length variants in semi-solid agar. (A) Motility performance of chemotactic (che⁺) and (B) non-chemotactic (Δ*cheY*, che⁻) hook length mutants in semi-solid agar plates with varying agar concentrations (0.2%, 0.25%, 0.3%, 0.35% agar). The che⁺ mutants were incubated for 3-4 h whereas the che⁻ mutants were incubated for 14-18 h, depending on the agar concentration. For all panels, a representative motility plate is shown on the right-hand side. FliK length in amino acids is indicated; (–) annotates the non-flagellated control strain Δ*fliHIJ*. Individual replicates are shown and black bars represent the mean motility normalized to the wt. FliK mutants with uncontrolled hook length are highlighted in red.

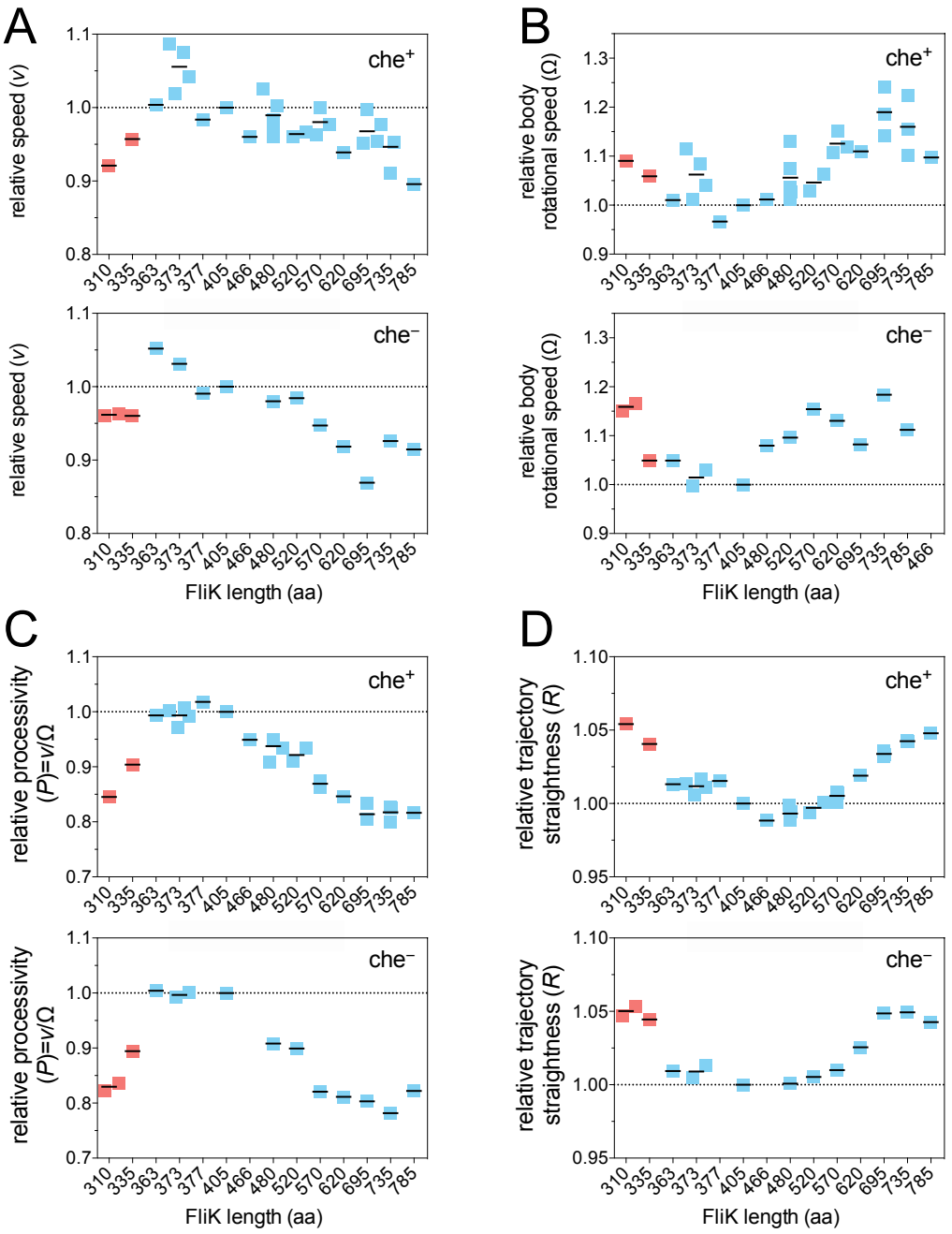

687

688 **Fig. 4: Motility performance of hook length mutants in 3D.** (A) Swimming speed *v*, (B)
689 body rotational speed Ω, (C) processivity $P=v/\Omega$, (D) straightness of trajectory *R*. Data
690 points represent individual experiments normalized to the wt (black bars; mean).
691 Uncontrolled hook length mutants are shown in red. All parameters were obtained by
692 normalizing the time-dependent parameters to the wt (FliK405) and by averaging over the
693 time-window 10 min<t<60 min.

694 **Supplementary Materials**

695 Supplementary Text S1-3

696 Supplementary Table S1

697 Supplementary Figs S1-S12

698 Supplementary Movie S1

Supplementary Text S1

Observations from modeling of single-cell behavior

The angular velocity ψ is related to the tangential velocity v and the radius s of the curvature of the cell trajectory as $\psi = {}^{v}/_{s}$, making this parameter proportional to the cell velocity and inversely proportional to the radius of curvature. We observed that the angular velocity initially increases with hook length. This corresponds to a decrease in the curvature radius of the trajectories, similar as observed before for sperm cells swimming near surfaces (47). The angular velocity ψ decreases for longer trajectories, however, as a consequence of decreased run speed v. We also note that we were unable to reproduce the experimental observables of the short-hook ($FliK_{335}$) che^{-} mutant by a single parameter couple (ψ,λ) in the context of our run-and-tumble model, which suggested that the movement of those mutants is not diffusive (Supplementary Fig. S7). We suggest that the observed heterogeneous hook length distribution of the $FliK_{335}$ mutant (Supplementary Fig. S3) explains the poor fit to a single parameter couple.

Supplementary Text S2

Derivation of the velocity autocorrelation function for the circular run-and-tumble model

First, we start by defining the model. This is a true minimal model. We assume that bacteria can be regarded as point particles moving in two dimensions, along perfect circles, with a constant tangential speed. The angular velocity with which bacteria move along their circular path is ν. Choosing the units such that the radius of the circular trajectory is unitary $s = 1$, the trajectory of an individual bacterium can be parametrized with time t as

(1) $$\vec{r}(t) = (\cos \nu t\,, \sin \nu t)$$

Correspondingly, the velocity of the bacterium $\vec{v}(t) = \frac{d\vec{r}}{dt}$ is

(2) $$\vec{v}(t) = v(-\sin \nu t\,, \cos \nu t)$$

From Eq. 2, we see that the initial velocity of the bacterium is

(3) $$\vec{v}(0) = (0, \nu).$$

Next, we assume that after some time τ_1 has passed, the bacterium will tumble and start moving along a different circle of the same radius and with the same angular velocity, i.e. the velocity will be changed by a phase shift $\phi_i \in [0,2\pi)$. We assume that tumbles can make the bacterium reorient towards any possible direction, and that the reorientations after each tumble are independent of one another (Markov property) i.e. ϕ_i, $i \in \mathbb{N}$ are stochastic variables distributed as

(4) $$P(\phi_i) = \frac{1}{2\pi}.$$

We also assume that the intertumbling times τ_i, $i \in \mathbb{N}$ are completely independent of each other, i.e. the intertumbling times are stochastic variables distributed as

(5) $$P(\tau_i) = \lambda e^{-\lambda \tau_i},$$

where the parameter $\lambda > 0$ of the distribution is known as the tumbling rate.

The angular autocorrelation, defined as

(6) $$g(t) = \frac{\vec{v}(0) \cdot \vec{v}(t)}{|\vec{v}(0)||\vec{v}(t)|},$$

is a measure of the similarity of the initial velocity of the bacterium and its velocity at a later time t. Even though strictly speaking, the velocity of the bacterium at time t is given by the expression

$$\vec{v}(t) = \nu\left(-\sin\left(\nu t + \sum_i \Theta(t - \tau_i)\phi_i\right), \cos\left(\nu t + \sum_i \Theta(t - \tau_i)\phi_i\right)\right),$$

where $\Theta(x)$ is the Heaviside function, due to the Markov property and statistical properties of the phase shifts ϕ_i, and for the purposes of calculating the angular correlation this expression can be rewritten as

(7) $$\vec{v}(t) = v(-\sin(vt + \xi\phi), \cos(vt + \xi\phi)),$$

where $\phi =: \phi_1 + \sum_{i=2} \Theta(t - \tau_i)\phi_i$ is an effective phase shift, distributed following Eq. 4 and

(8) $$\xi := \Theta(t - \tau_1)$$

is a stochastic Boolean variable, $\xi \in \{0,1\}$.

The stochastic variable ξ has a value of $\xi = 0$ if the bacterium has not tumbled for the first time, and $\xi = 1$ if it has tumbled at least once. From Eqs. 5 and 8, it is evident that the probability of $\xi = 1$ is just the cumulative distribution function of τ_i, that is

(9) $$P(\xi = 1) = 1 - e^{-\lambda t}, \text{ and}$$

(10) $$P(\xi = 0) = e^{-\lambda t}$$

From Eqs. 3, 6, and 7 we have the following

$$g(t) = \frac{\vec{v}(0)\cdot\vec{v}(t)}{|\vec{v}(0)||\vec{v}(t)|}$$

$$= \frac{v^2 \cos(vt+\xi\phi)}{v^2}$$

$$= \cos(vt + \xi\phi).$$

The velocity autocorrelation function is defined as the expected value of the angular autocorrelation, $\langle g(t)\rangle$. Therefore, in this model, the velocity autocorrelation fucntion is given by

(11) $$\langle g(t)\rangle = \langle \cos(vt + \xi\phi)\rangle,$$

where the average is performed over all possible values of ϕ and ξ.

Due to the simplicity of the angular autocorrelation and probability distributions, the velocity autocorrelation function can be calculated analytically using trigonometric identities, Eqs. 4, 9, and 10, as follows

$$\langle g(t)\rangle = \langle \cos(vt + \xi\phi)\rangle$$

$$= \int_0^{2\pi} \left[\sum_{\xi=0}^{1} \cos(\nu t + \xi\phi)\, P(\xi) \right] P(\phi) d\,\phi$$

$$= \cos(\nu t) \int_0^{2\pi} \left[\sum_{\xi=0}^{1} \cos(\xi\phi)\, P(\xi) \right] P(\phi) d\,\phi$$

$$- \sin(\nu t) \int_0^{2\pi} \left[\sum_{\xi=0}^{1} \sin(\xi\phi)\, P(\xi) \right] P(\phi) d\,\phi$$

$$= \frac{\cos(\nu t)}{2\pi} \int_0^{2\pi} \left[e^{-\lambda t} + \left(1 - e^{-\lambda t}\right) \cos\phi \right] d\,\phi$$

$$- \frac{\sin(\nu t)}{2\pi} \int_0^{2\pi} \left(1 - e^{-\lambda t}\right) \sin\phi d\,\phi$$

$$= \frac{\cos(\nu t)}{2\pi} \left[e^{-\lambda t} \phi|_0^{2\pi} + \left(1 - e^{-\lambda t}\right) \underbrace{\sin\phi|_0^{2\pi}}_{=0} \right]$$

$$+ \frac{\sin(\nu t)}{2\pi} \left(1 - e^{-\lambda t}\right) \underbrace{\cos\phi|_0^{2\pi}}_{=0}$$

$$= \cos(\nu t)\, e^{-\lambda t}.$$

Therefore, in this simple model, the velocity autocorrelation function is given by

$$\langle g(t) \rangle = \cos(\nu t)\, e^{-\lambda t}.$$

Supplementary Text S3

Effects of growth medium and temperature on single-cell behavior

For experimental reasons, single cell tracking in quasi 2D was performed with cells grown in LB medium at 37 °C, whereas bacteria for the DDM and DFM experiments were grown in TB medium at 30 °C. While the overall motility behavior was remarkably similar between the experimental conditions (Fig. 2, Fig. 4, Supplementary Fig. S9), we observed a substantial decrease in swimming speed for long hook mutants grown in LB at 37 °C. These differences may be attributed to increased flagella numbers per cell for bacteria grown in LB at 37 °C, which presumably exacerbate the increased bundle instability of the long hook mutants (Supplementary Fig. S9).

805 # Supplementary Tables

806 **Supplementary Table S1.** List of *Salmonella* Typhimurium strains used in this study.

Strain	Genotype	Reference
EM2634	*fliK*22363 (Δaa63-157) FliK310	This study
EM2655	*fliK*22364 (Δaa127-169) FliK335	This study
TH9545	*fliK*6436 (Δaa161-202) FliK363	This study
TH10335	*fliK*6619 (Δaa238-269) FliK373	This study
TH9543	*fliK*6434 (Δaa161-188) FliK377	This study
TH437	LT2 wild type FliK405	John Roth
TH9798	*fliK*6529 (*fliK*180'-YscP(321-381)-'181*fliK*) FliK466	This study
TH8259	*fliK*6128 (*fliK*140'-YscP(307-381)-'141*fliK*) FliK480	This study
TH9795	*fliK*6526(*fliK*140'-YscP(146-260)-'141*fliK*) FliK520	This study
TH8258	*fliK*6127(*fliK*140'-YscP(217-381)-'141*fliK*) FliK570	This study
EM2799	*fliK*22381 (*fliK*95'-YscP(138-353)-'96*fliK*) FliK620	This study
EM2797	*fliK*22379 (*fliK*95'-YscP(138-353)-'96*fliK* + *fliK*140'-YscP(307-381)-'141*fliK*) FliK695	This study
EM2798	*fliK*22380 (*fliK*95'-YscP(138-353)-'96*fliK* + *fliK*140'-YscP(146-260)-'141fliK) FliK735	This study
EM2796	*fliK*22378 (*fliK*95'-YscP(138-353)-'96*fliK* + *fliK*140'-YscP(217-381)-'141fliK) FliK785	This study
TH12427	Δ*fliHIJ*7367	Lab stock
EM4083	*fliK*22363 (Δaa63-157) Δ*hin*-5717::FCF (fliC-ON) FliK310	This study
EM4082	*fliK*22364 (Δaa127-169) Δ*hin*-5717::FCF (fliC-ON) FliK335	This study
EM4081	*fliK*6436 (Δaa161-202) Δ*hin*-5717::FCF (fliC-ON) FliK363	This study
EM4084	*fliK*6619 (Δaa238-269) Δ*hin*-5717::FCF (fliC-ON) FliK373	This study
EM4078	*fliK*6434 (Δaa161-188) Δ*hin*-5717::FCF (fliC-ON) FliK377	This study
TH5861	Δ*hin*-5717::FCF (fliC-ON) FliK405	Lab stock
EM4077	*fliK*6529 (*fliK*180'-YscP(321-381)-'181*fliK*) Δ*hin*-5717::FCF (fliC-ON) FliK466	This study
EM4085	*fliK*6128 (*fliK*140'-YscP(307-381)-'141*fliK*) Δ*hin*-5717::FCF (fliC-ON) FliK480	This study
EM4080	*fliK*6526(*fliK*140'-YscP(146-260)-'141*fliK*) Δ*hin*-5717::FCF (fliC-ON) FliK520	This study
EM4079	*fliK*6127(*fliK*140'-YscP(217-381)-'141*fliK*) Δ*hin*-5717::FCF (fliC-ON)	This study

	FliK570	
EM4087	*fliK*22381 (*fliK*95'-YscP(138-353)-'96*fliK*) Δ*hin*-5717::FCF (fliC-ON) FliK620	This study
EM4086	*fliK*22379 (*fliK*95'-YscP(138-353)-'96*fliK* + *fliK*140'-YscP(307-381)-'141*fliK*) Δ*hin*-5717::FCF (fliC-ON) FliK695	This study
EM4088	*fliK*22380 (*fliK*95'-YscP(138-353)-'96*fliK* + *fliK*140'-YscP(146-260)-'141fliK) Δ*hin*-5717::FCF (fliC-ON) FliK735	This study
EM4089	*fliK*22378 (*fliK*95'-YscP(138-353)-'96*fliK* + *fliK*140'-YscP(217-381)-'141fliK) Δ*hin*-5717::FCF (fliC-ON) FliK785	This study
EM4091	Δ*fliHIJ*7367 Δ*hin*-5717::FCF (fliC-ON)	This study
EM3004	*fliK*22363 (Δaa63-157) P*flhDC*5451::Tn*10d*Tc[del-25]/ pRG19 FliK310	This study
EM3005	*fliK*22364 (Δaa127-169) P*flhDC*5451::Tn*10d*Tc[del-25]/ pRG19 FliK335	This study
EM3013	*fliK*6436 (Δaa161-202) $P_{flhDC5451}$::Tn*10d*Tc[del-25] [a)]/ pRG19 FliK363	This study
EM3012	*fliK*6619 (Δaa238-269) $P_{flhDC5451}$::Tn*10d*Tc[del-25] [a)]/ pRG19 FliK373	This study
EM3006	*fliK*6434 (Δaa161-188) $P_{flhDC5451}$::Tn*10d*Tc[del-25] [a)]/ pRG19 FliK377	This study
EM2999	$P_{flhDC5451}$::Tn*10d*Tc[del-25] [a)]/ pRG19 FliK405	This study
EM3003	*fliK*6529 (*fliK*180'-YscP(321-381)-'181*fliK*) $P_{flhDC5451}$::Tn*10d*Tc[del-25] [a)]/ pRG19 FliK466	This study
EM3002	*fliK*6128 (*fliK*140'-YscP(307-381)-'141*fliK*) $P_{flhDC5451}$::Tn*10d*Tc[del-25] [a)]/ pRG19 FliK480	This study
EM3001	*fliK*6526(*fliK*140'-YscP(146-260)-'141*fliK*) $P_{flhDC5451}$::Tn*10d*Tc[del-25] [a)]/ pRG19 FliK520	This study
EM3000	*fliK*6127(*fliK*140'-YscP(217-381)-'141*fliK*) $P_{flhDC5451}$::Tn*10d*Tc[del-25] [a)]/ pRG19 FliK570	This study
EM3007	*fliK*22381 (*fliK*95'-YscP(138-353)-'96*fliK*) $P_{flhDC5451}$::Tn*10d*Tc[del-25] [a)]/ pRG19 FliK620	This study
EM3009	*fliK*22379 (*fliK*95'-YscP(138-353)-'96*fliK* + *fliK*140'-YscP(307-381)-'141*fliK*) $P_{flhDC5451}$::Tn*10d*Tc[del-25] [a)]/ pRG19 FliK695	This study
EM3010	*fliK*22380 (*fliK*95'-YscP(138-353)-'96*fliK* + *fliK*140'-YscP(146-260)-'141fliK) $P_{flhDC5451}$::Tn*10d*Tc[del-25] [a)]/ pRG19 FliK735	This study
EM3008	*fliK*22378 (*fliK*95'-YscP(138-353)-'96*fliK* + *fliK*140'-YscP(217-381)-'141fliK) $P_{flhDC5451}$::Tn*10d*Tc[del-25] [a)]/ pRG19 FliK785	This study
EM3011	Δ*fliHIJ*7367 $P_{flhDC5451}$::Tn*10d*Tc[del-25] [a)]/ pRG19	This study
EM2912	*fliK*22363 (Δaa63-157) Δ*cheY*22371::FKF FliK310	This study
EM2911	*fliK*22364 (Δaa127-169) Δ*cheY*22371::FKF FliK335	This study

EM2913	*fliK*6436 (Δaa161-202) Δ*cheY*22371::FKF FliK363	This study
EM2914	*fliK*6619 (Δaa238-269) Δ*cheY*22371::FKF FliK373	This study
EM2915	*fliK*6434 (Δaa161-188) Δ*cheY*22371::FKF FliK377	This study
EM2916	Δ*cheY*22371::FKF FliK405	This study
EM2917	*fliK*6529 (*fliK*180'-YscP(321-381)-'181*fliK*) Δ*cheY*22371::FKF FliK466	This study
EM2918	*fliK*6128 (*fliK*140'-YscP(307-381)-'141*fliK*) Δ*cheY*22371::FKF FliK480	This study
EM2919	*fliK*6526(*fliK*140'-YscP(146-260)-'141*fliK*) Δ*cheY*22371::FKF FliK520	This study
EM2920	*fliK*6127(*fliK*140'-YscP(217-381)-'141*fliK*) Δ*cheY*22371::FKF FliK570	This study
EM2921	*fliK*22381 (*fliK*95'-YscP(138-353)-'96*fliK*) Δ*cheY*22371::FKF Δ*cheY*22371::FKF FliK620	This study
EM2922	*fliK*22379 (*fliK*95'-YscP(138-353)-'96*fliK* + *fliK*140'-YscP(307-381)-'141*fliK*) Δ*cheY*22371::FKF FliK695	This study
EM2923	*fliK*22380 (*fliK*95'-YscP(138-353)-'96*fliK* + *fliK*140'-YscP(146-260)-'141fliK) Δ*cheY*22371::FKF FliK735	This study
EM2924	*fliK*22378 (*fliK*95'-YscP(138-353)-'96*fliK* + *fliK*140'-YscP(217-381)-'141fliK) Δ*cheY*22371::FKF FliK785	This study
EM2925	Δ*fliHIJ*7367 Δ*cheY*22371::FKF	This study
EM4649	*fliK*22363 (Δaa63-157) Δ*invH*-sprB::FKF FliK310	This study
EM3966	*fliK*22364 (Δaa127-169) Δ*invH*-sprB::FKF FliK335	This study
EM2020	*fliK*6436 (Δaa161-202) Δ*invH*-sprB::FKF FliK363	This study
EM2024	*fliK*6619 (Δaa238-269) Δ*invH*-sprB::FKF FliK373	This study
EM2019	*fliK*6434 (Δaa161-188) Δ*invH*-sprB::FKF FliK377	This study
TH16133	Δ*invH*-sprB::FKF	Lab stock
EM4650	*fliK*6529 (*fliK*180'-YscP(321-381)-'181*fliK*) Δ*invH*-sprB::FKF FliK466	This study
EM2016	*fliK*6128 (*fliK*140'-YscP(307-381)-'141*fliK*) Δ*invH*-sprB::FKF FliK480	This study
EM2022	*fliK*6526(*fliK*140'-YscP(146-260)-'141*fliK*) Δ*invH*-sprB::FKF FliK520	This study
EM2015	*fliK*6127(*fliK*140'-YscP(217-381)-'141*fliK*) Δ*invH*-sprB::FKF FliK570	This study
EM3968	*fliK*22381 (*fliK*95'-YscP(138-353)-'96*fliK*) Δ*invH*-sprB::FKF FliK620	This study
EM4004	*fliK*22379 (*fliK*95'-YscP(138-353)-'96*fliK* + *fliK*140'-YscP(307-381)-'141*fliK*) Δ*invH*-sprB::FKF FliK695	This study
EM4005	*fliK*22380 (*fliK*95'-YscP(138-353)-'96*fliK* + *fliK*140'-YscP(146-260)-'141fliK) Δ*invH*-sprB::FKF FliK735	This study
EM3967	*fliK*22378 (*fliK*95'-YscP(138-353)-'96*fliK* + *fliK*140'-YscP(217-381)-'141fliK) Δ*invH*-sprB::FKF FliK785	This study
TH16562	Δ*fliHIJ*7367 Δ*invH*-sprB::FKF	Lab stock

807 [a)] Expression of *flhDC* under control of the anhydrotetracycline-inducible promoter P_{tetA}.

808 **Supplementary Figures**

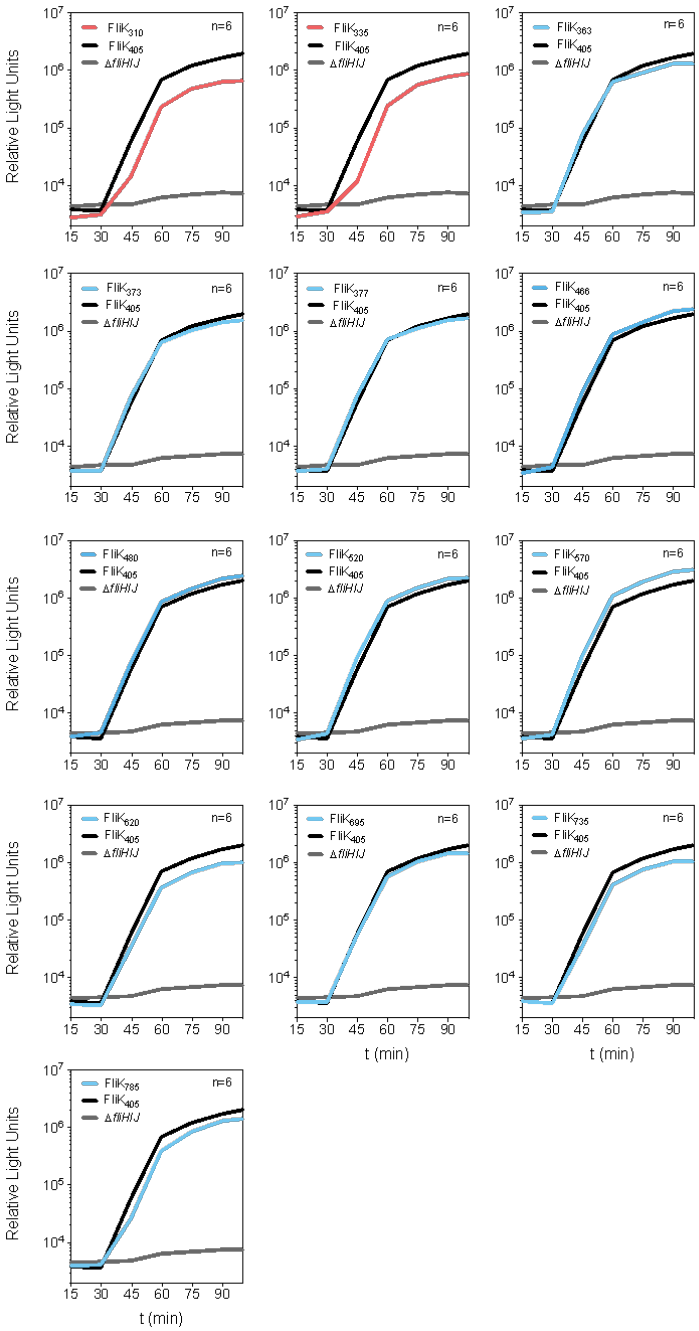

809

810 **Supplementary Fig. S1: Substrate secretion switch of the hook length mutants.**
811 Expression of flagella synthesis was synchronized by induction of the P_{tetA}-*flhDC* flagellar
812 master regulatory operon. The switch in secretion specificity was monitored over time by
813 measuring promoter activity of a Class 3 P_{motA}-*luxCDABE* reporter. Individual panels
814 compare a hook length mutant (FliK length indicated in aa), the wt (FliK405) and the
815 negative control (Δ*fliHIJ*). Uncontrolled hook length mutants are shown in red.

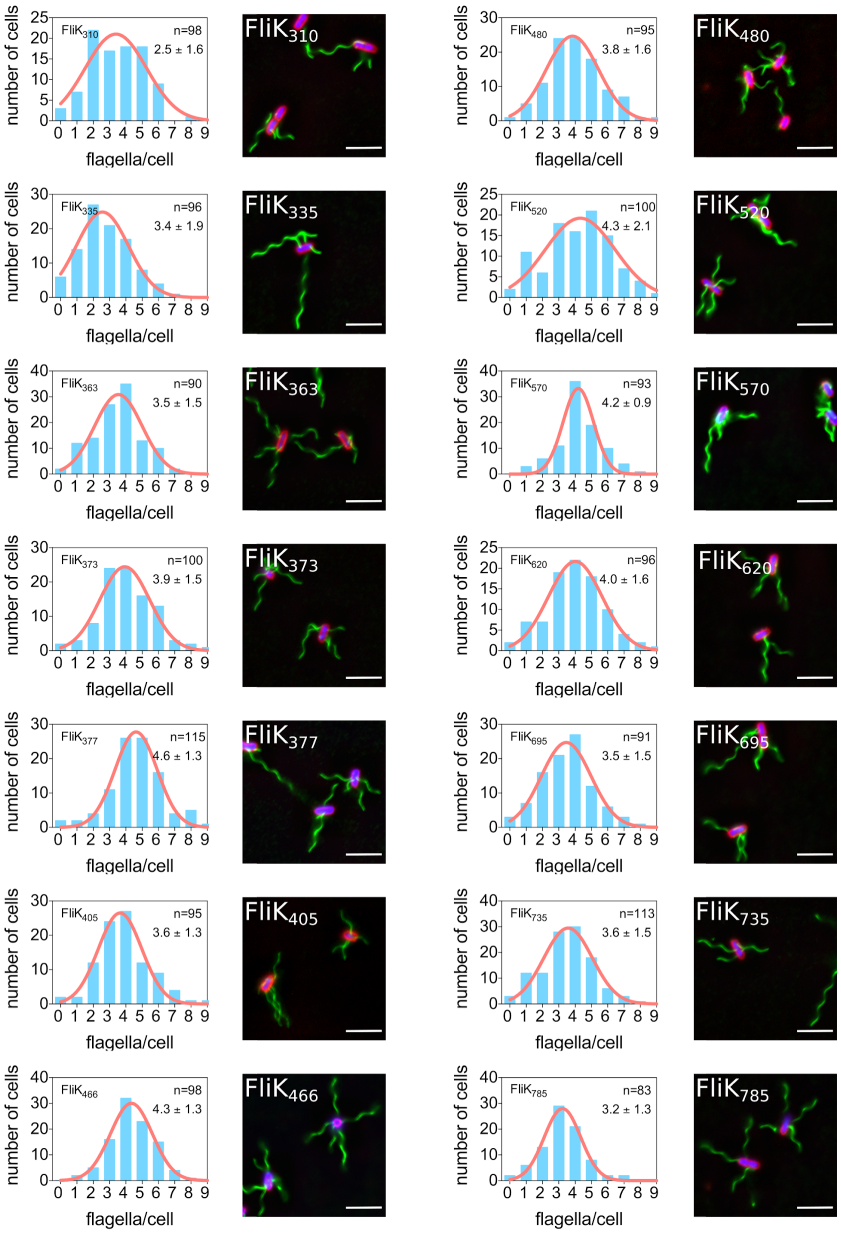

Supplementary Fig. S2: Hook mutants express the same number of flagella. (A) Quantification of the number of flagella of individual bacteria grown in LB at 37 °C. The flagellation pattern was determined by anti-flagellin immunostaining. Per mutant, the flagella per cell of all bacteria in 10 separate fields of view were counted manually. The average number of flagella per cell ± s.d. was calculated using Gaussian non-linear regression analysis. (B) Representative fluorescent microscopy images of anti-flagellin immunostaining. The flagellar filament was detected using anti-FliC immunostaining (green), membranes were stained using FM-64 (red) and DNA was stained using DAPI (blue). Scale bar = 5 μm.

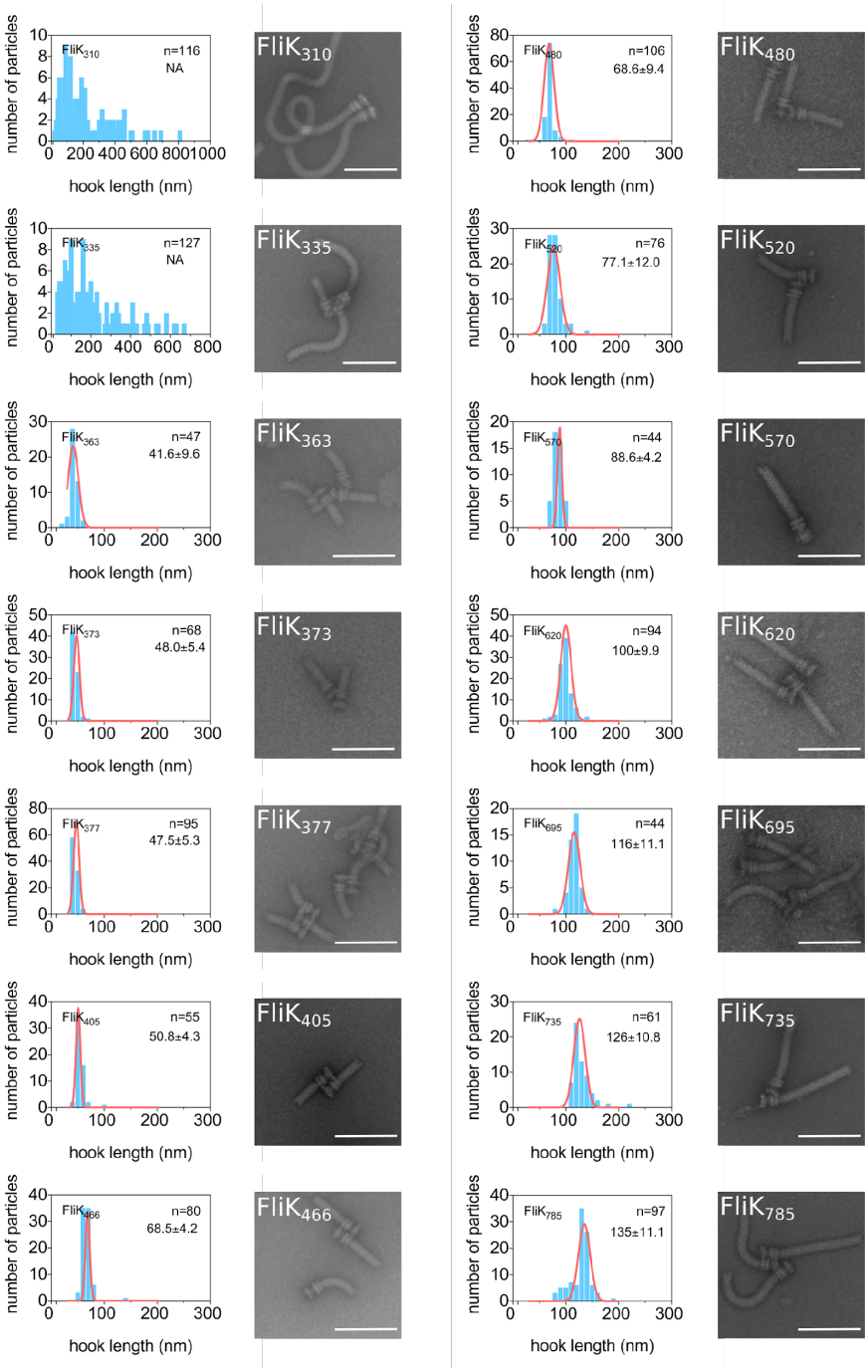

Supplementary Fig. S3: Hook length corresponds with FliK protein length. (A) Histograms of hooks isolated from the FliK mutants. Hook-basal-body complexes were purified and imaged by negative staining electron microscopy. The average hook length ± s.d. was calculated using Gaussian non-linear regression analysis. (B) Representative electron micrograph images of purified hook-basal-body complexes. Scale bar = 100 nm.

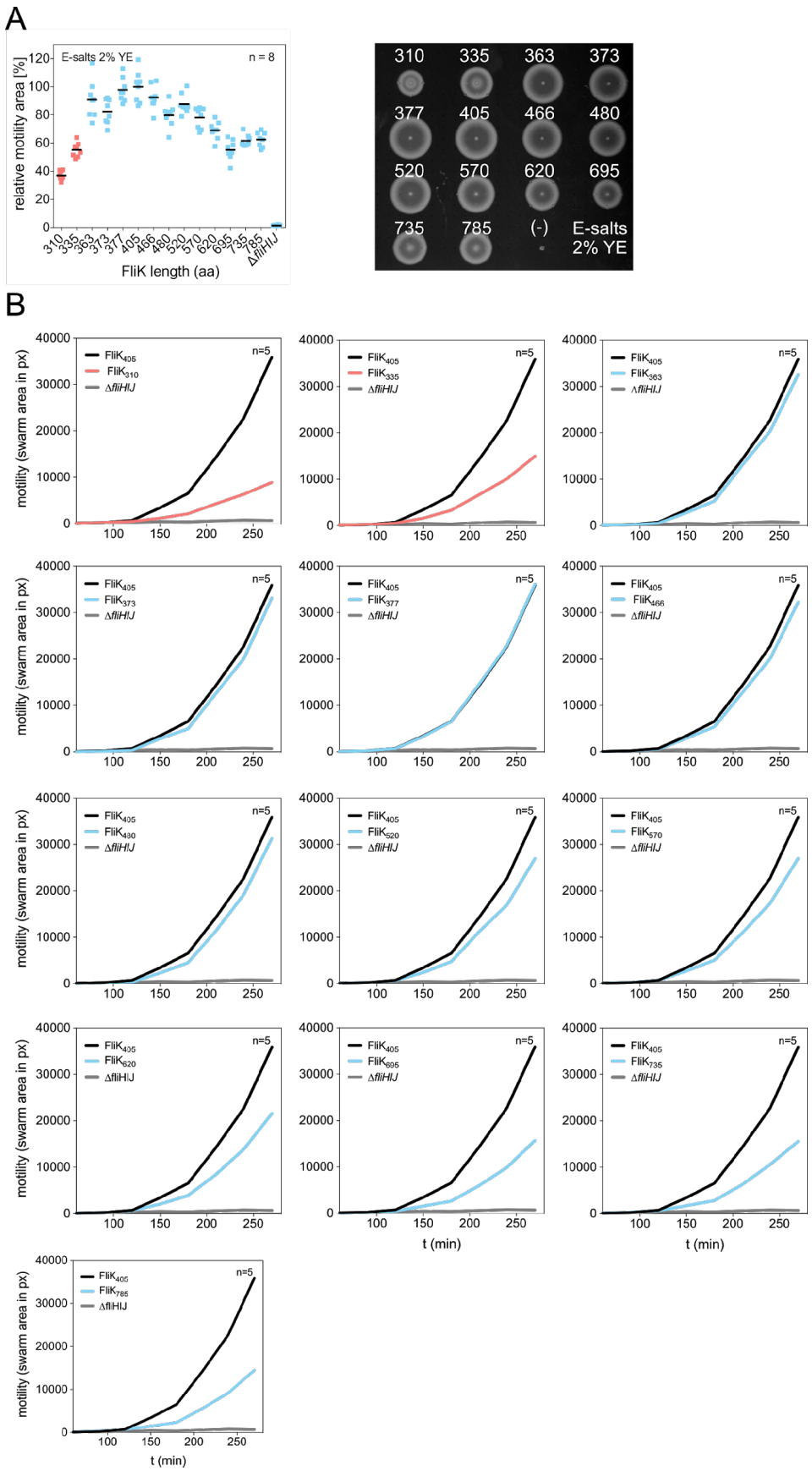
A
E-salts 2% YE
n = 8
relative motility area [%]
FliK length (aa)
310
335
363
373
377
405
466
480
520
570
620
695
735
785
ΔfliHIJ
(-)
E-salts 2% YE
B
motility (swarm area in px)
t (min)
n=5
FliK405
FliK310
FliK335
FliK363
FliK373
FliK377
FliK466
FliK480
FliK520
FliK570
FliK620
FliK695
FliK735
FliK785
ΔfliHIJ

832

833 **Supplementary Fig. S4: Swimming motility plate behavior of hook length variants.**
834 (A) Motility assay of the hook length mutants in minimal media 0.3% soft agar plates
835 containing 2% yeast extract. Quantification of the swimming motility assay (left panel) and
836 representative soft agar plate (right panel). FliK length in amino acids is indicated; (-)
837 indicates the non-flagellated control strain Δ*fliHIJ*. Motility halo size was measured using
838 ImageJ and normalized to the wt (dots represent single data points; bars represent the
839 mean; red dots represent the uncontrolled hook length mutants). (B) Time course motility
840 assay of the hook length mutants in 0.3% swimming motility agar plates. Motility halo size
841 was determined every 30 minutes and the average motility halo area of 5 biological
842 replicates is shown. Uncontrolled hook length mutants are shown in red.

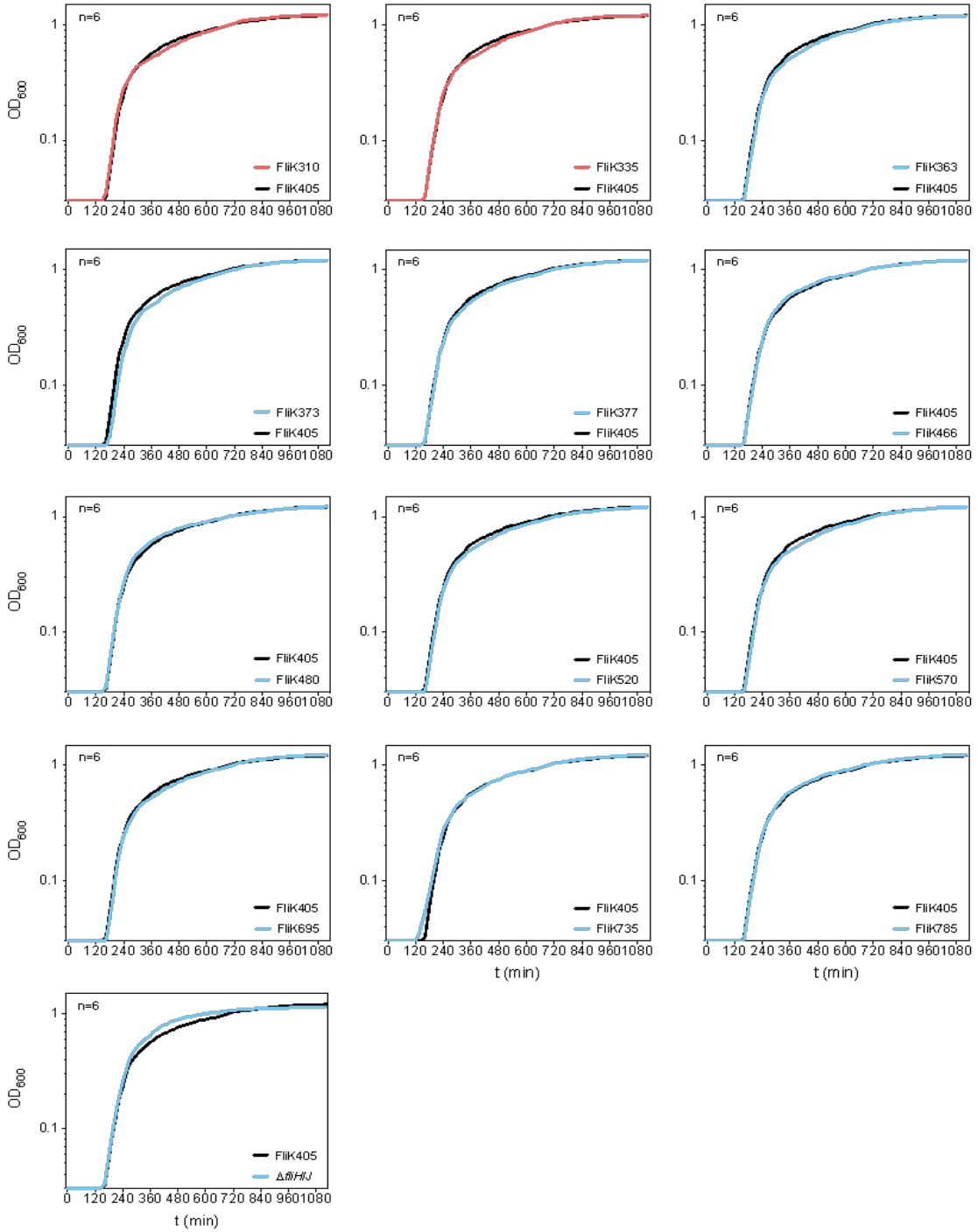

843

844 **Supplementary Fig. S5: Growth analysis of the hook length variants.** Bacteria were
845 cultured in liquid LB medium and the OD_{600} was measured every 15 minutes. The average
846 OD_{600} of 6 biological replicates is shown. Uncontrolled hook length mutants are shown in
847 red.

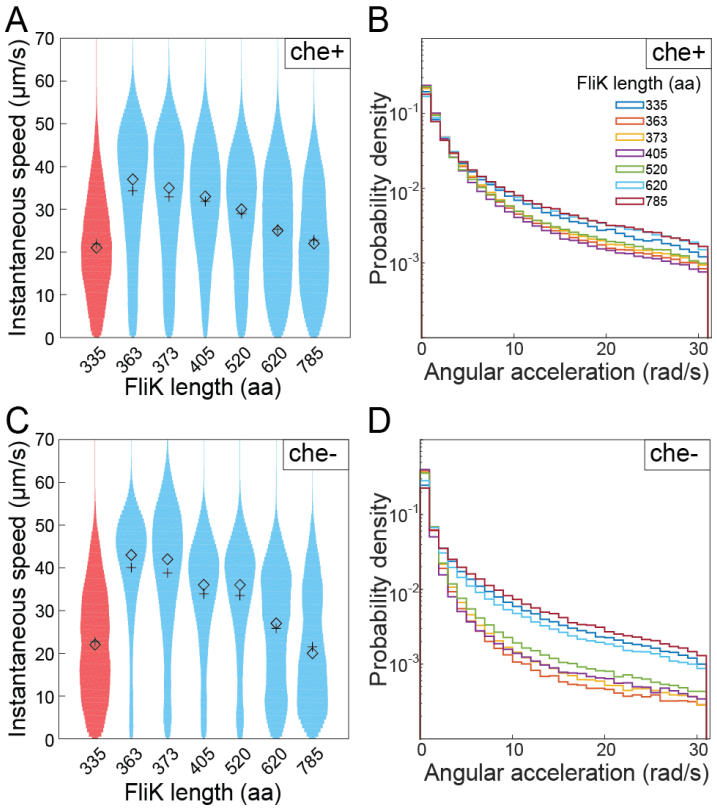

Supplementary Fig. S6: Motility performance of hook length variants in quasi 2D. The distributions of motility parameters for different hook-length mutants. Distributions of (A) the instantaneous speeds and (B) the angular velocities pooled from all the trajectories from cells with a WT genetic background (che+). (C-D) The same distributions from smooth swimming mutants due to deletion of *cheY* (che-). Each distribution was calculated from more than 1,000 minutes of cumulative trajectory times pooled from three independent biological replicates each containing more than 600 individual cells. Mean: +, median: ◊.

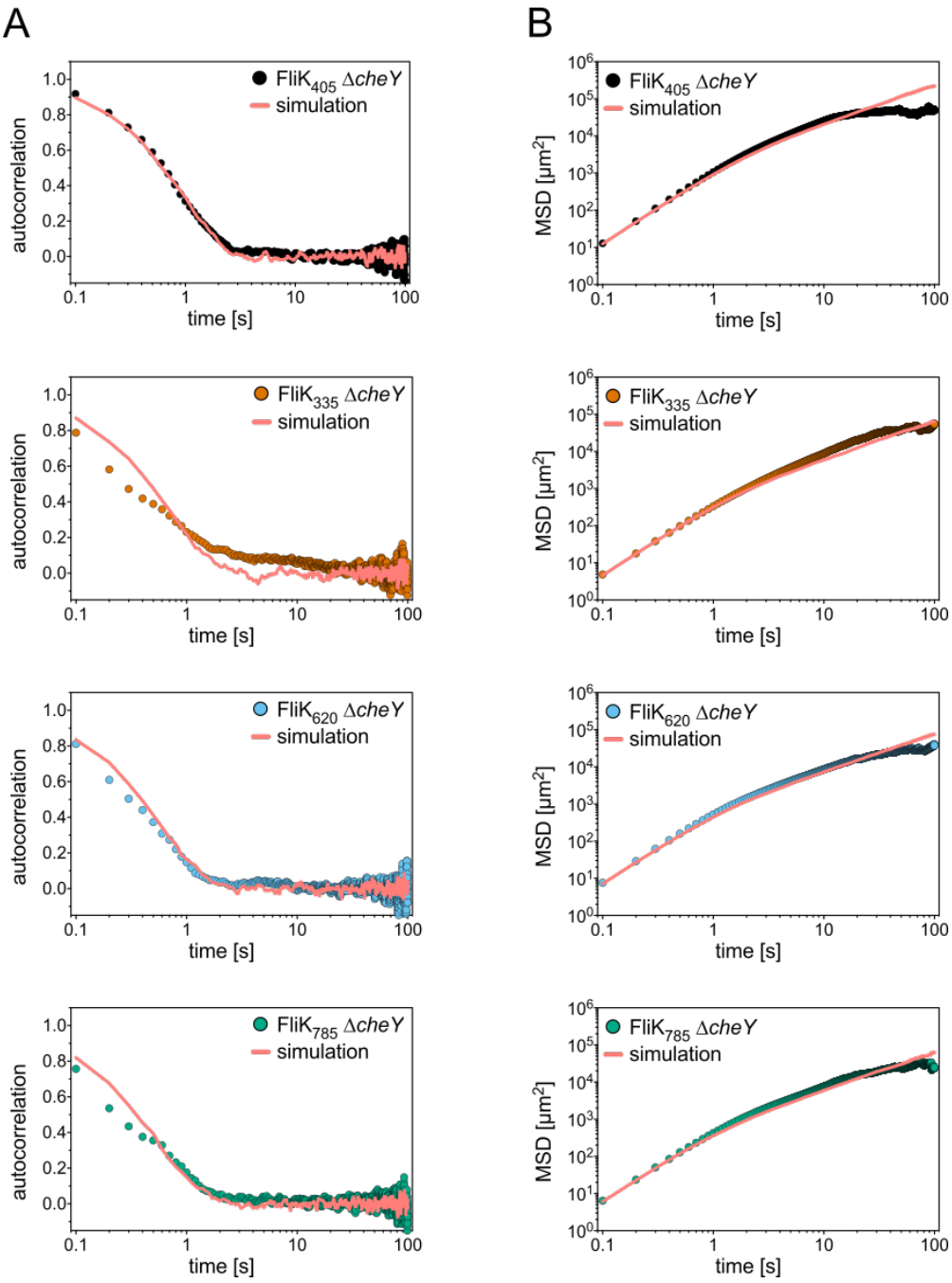

Supplementary Fig. S7: Autocorrelation functions and mean square displacement fits of the circular run-and-tumble model for selected hook length mutants. Observed orientational autocorrelation functions and circular run-and-tumble model autocorrelation function fits (A) and observed mean square displacements and circular run-and-tumble model mean square displacement fits (B) of chemotaxis deficient mutants (Δ*cheY*). Wt (FliK405) hook length is shown at the top. Hook length increases from top to bottom. The parameters of the model in each case are those reported in the supplementary text (Supplementary Text S2).

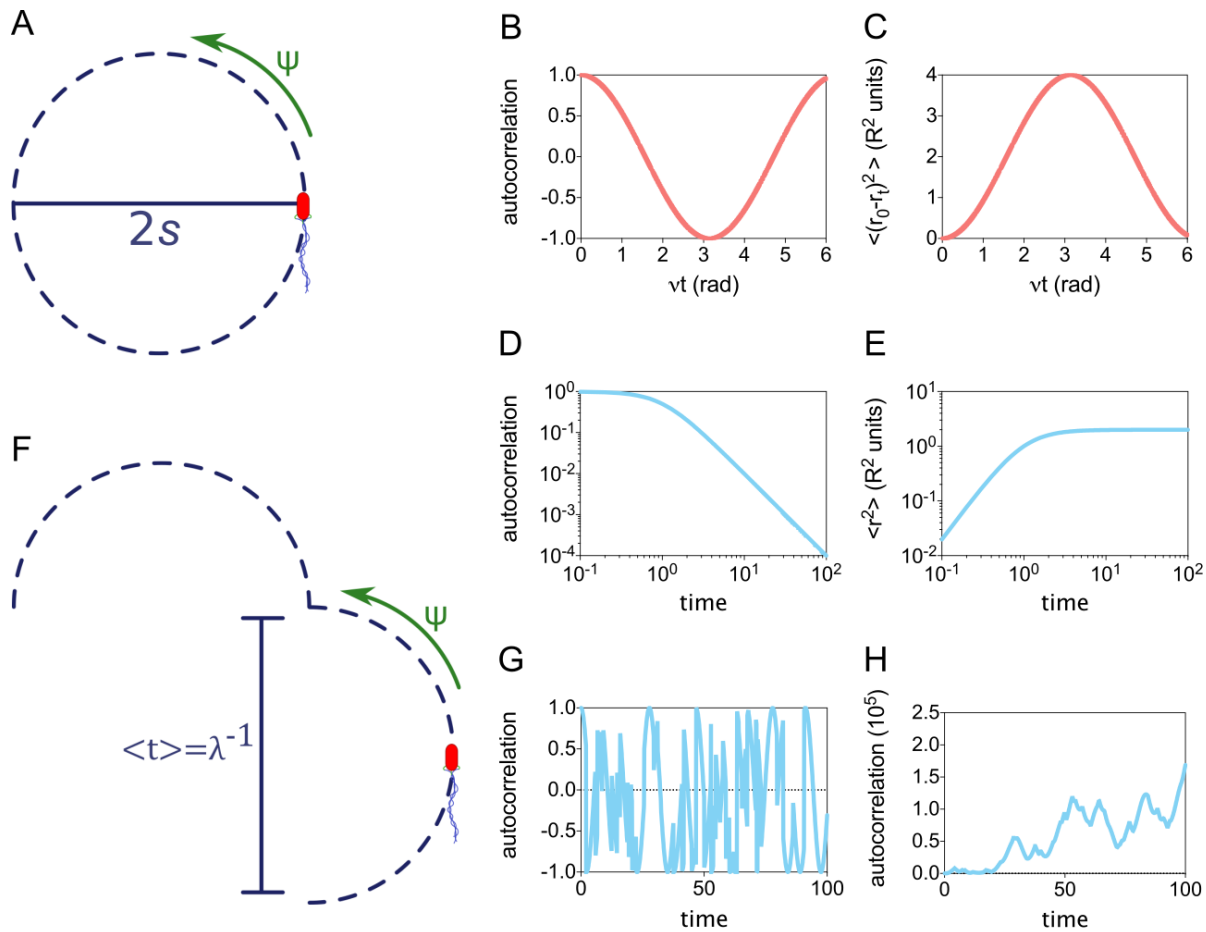

Supplementary Fig. S8: Circular run-and-tumble model. (A) In this model, individual cells are assumed to move on a circle of radius *s* with an angular velocity ψ. Under these conditions, the autocorrelation will be given by $\langle \overrightarrow{c_0} \cdot \overrightarrow{c_t} \rangle = \cos(\psi t)$. (B) and the mean square displacement will be given by $\langle r^2 \rangle = 2s^2[1 - \cos(\psi t)]$ (C). (D) Autocorrelation function and (E) mean square displacement under the assumption that the angular velocities are distributed among the population according to *P*(ψ). Shown are the observables when $P(\psi) = \lambda e^{-\lambda\psi}$. (F) Sample track of a virtual cell in the circular run-and-tumble model. The cell starts moving on a circle as in the uniform circular motion model; however, at exponentially distributed waiting times, the cell will reorient (tumble) and move along a new circular path. An example of autocorrelation of a single realization of the model is shown in panel G. An example of square displacement of a single realization of the model is shown in panel H. The value of the circular path radius s, necessary for the calculation of $\langle r^2 \rangle$ was obtained with the relation between the angular velocity ψ and tangential velocity *v*, $\psi = {}^{v}/_{s}$. The value of ψ was obtained from the fitting of the model to the experimentally observed autocorrelation function, while the value of the tangential velocity *v* was obtained from the first data point of the observed mean square displacement $\langle r^2 \rangle$ of each strain, by assuming ballistic movement at short times, *i.e.* $\langle r^2 \rangle \approx \langle v^2 \rangle t^2$, therefore $\langle v \rangle \approx \sqrt{\frac{\langle r^2 \rangle}{t^2}}$.

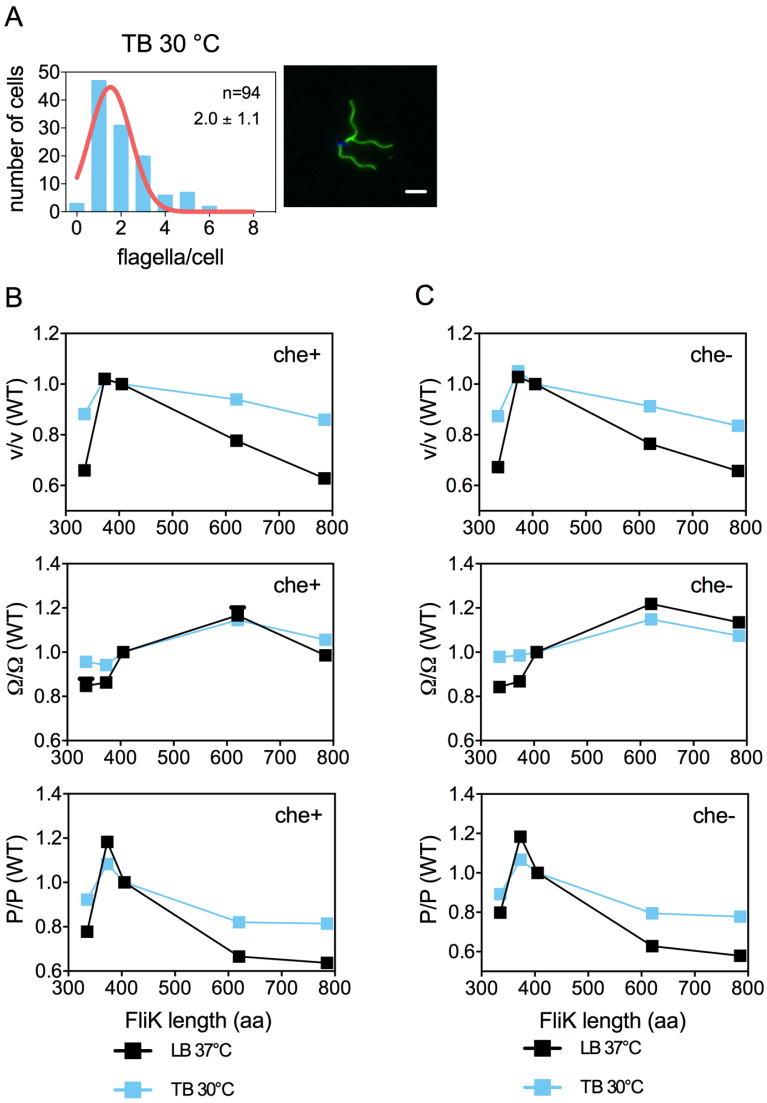

885

886 **Supplementary Fig. S9: Comparison of motility parameters under different**
887 **experimental conditions.** (A) Left: Quantification of the number of flagella of individual
888 bacteria grown in TB medium at 30 °C. The flagellation pattern was determined by anti-
889 flagellin immunostaining. The average number of flagella per cell ± s.d. was calculated
890 using Gaussian non-linear regression analysis. Right: Representative fluorescent
891 microscopy images of anti-flagellin immunostaining. The flagellar filament was detected
892 using anti-FliC immunostaining (green) and DNA was stained using DAPI (blue). (B)
893 Measurement of swimming speed v, body rotational speed Ω and processivity $P = v / \Omega$
894 relative to the wild type for hook length mutants grown in in LB at 37 °C and TB at 30 °C.
895 (C) Measurement of swimming speed v, body rotational speed Ω and processivity $P = v /$
896 Ω relative to the wild type for chemotactic deficient (Δ*cheY*) hook length mutants grown
897 in LB at 37 °C and TB at 30 °C.

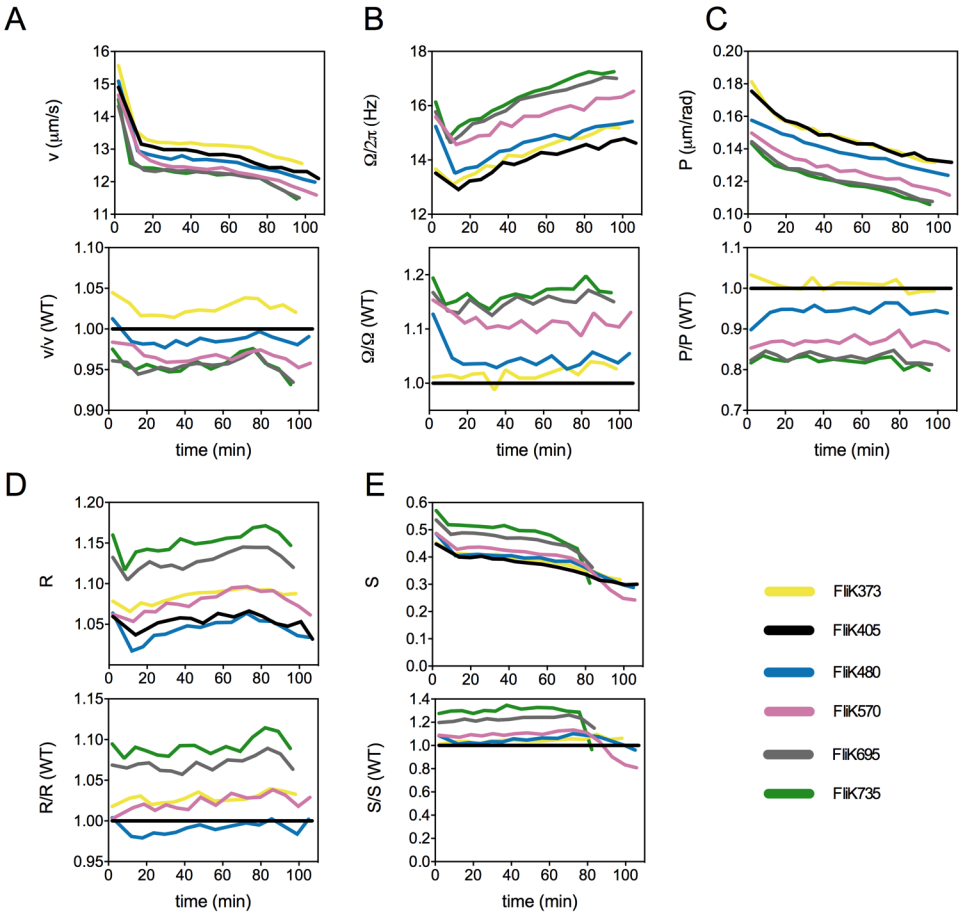

Supplementary Fig. S10: Time dependency of motility parameters for a single dataset. Absolute values (upper panels) and corresponding data normalized to the wt strain FliK405 (lower panels). (A) Swimming speed v, (B) body angular velocity Ω, (C) processivity $P = v / \Omega$, (D) straightness of trajectory R, (E) relative width S, of the speed distribution $P(v)$. Mean values presented in Fig. 4 are obtained by averaging over the time-window 10 min < t < 60 min.

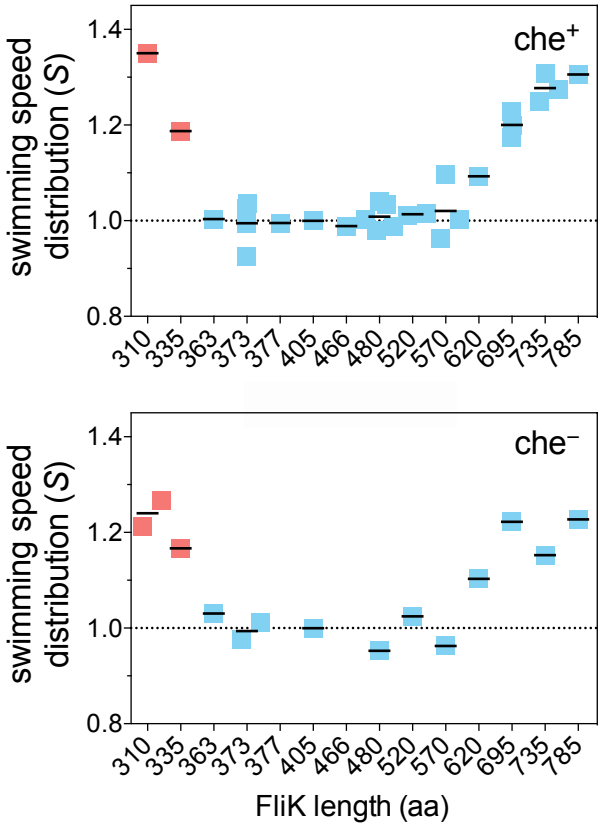

Supplementary Fig. S11: Relative width $S = \sigma / v$ of the speed distribution $P(v)$ of FliK mutants. Upper panel: FliK mutants capable of chemotaxis; Lower panel: smooth swimming FliK mutants due to deletion of *cheY*. Data points represent the mean of an average of up to 5 experiments and were normalized to the wt. Uncontrolled hook length mutants are shown in red.

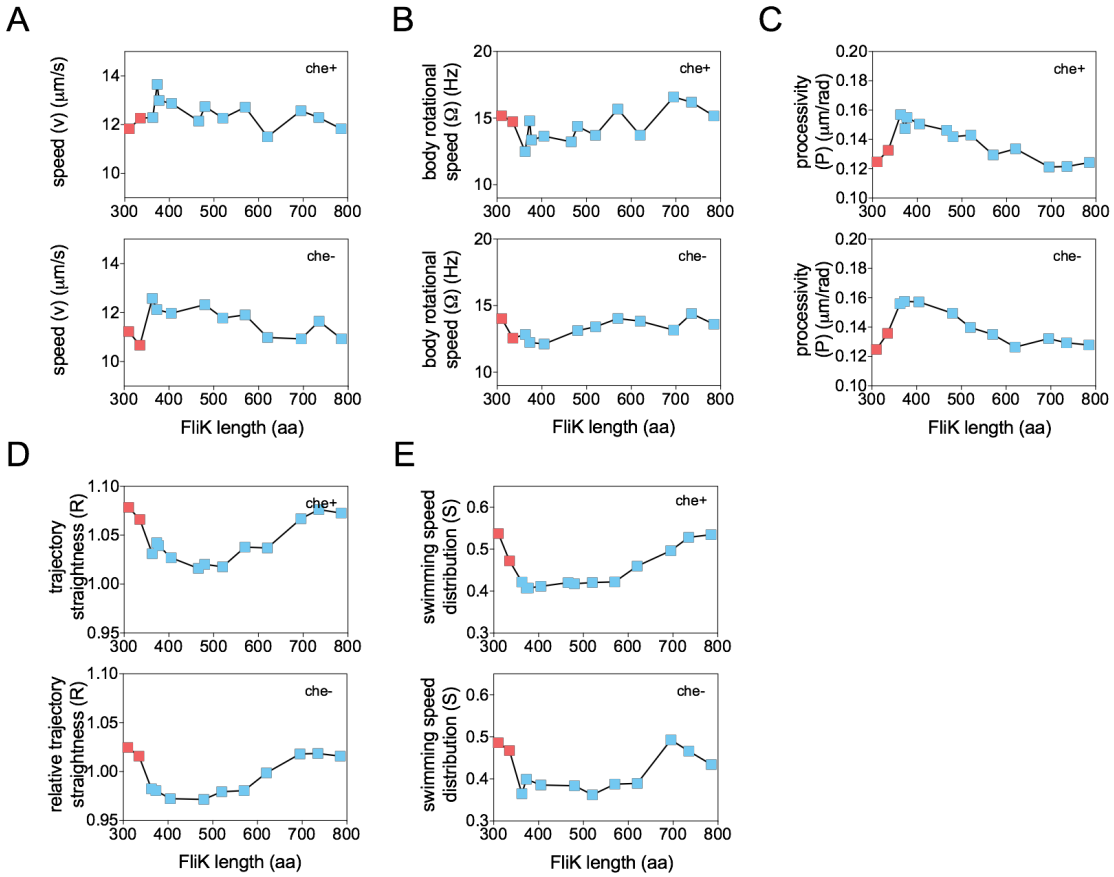

Supplementary Fig. S12: Representative data set of absolute values obtained from normalized quantities. (A) Swimming speed *v*, (B) body rotational speed *Ω*, (C) processivity $P = v / \Omega$, (D) straightness of trajectory *R*, (E) relative width *S*, of the speed distribution $P(v)$. Upper panel: FliK mutants capable of chemotaxis; Lower panel: smooth swimming FliK mutants due to deletion of *cheY*. Data points represent the mean of an average of up to 5 experiments. Uncontrolled hook length mutants are shown in red.

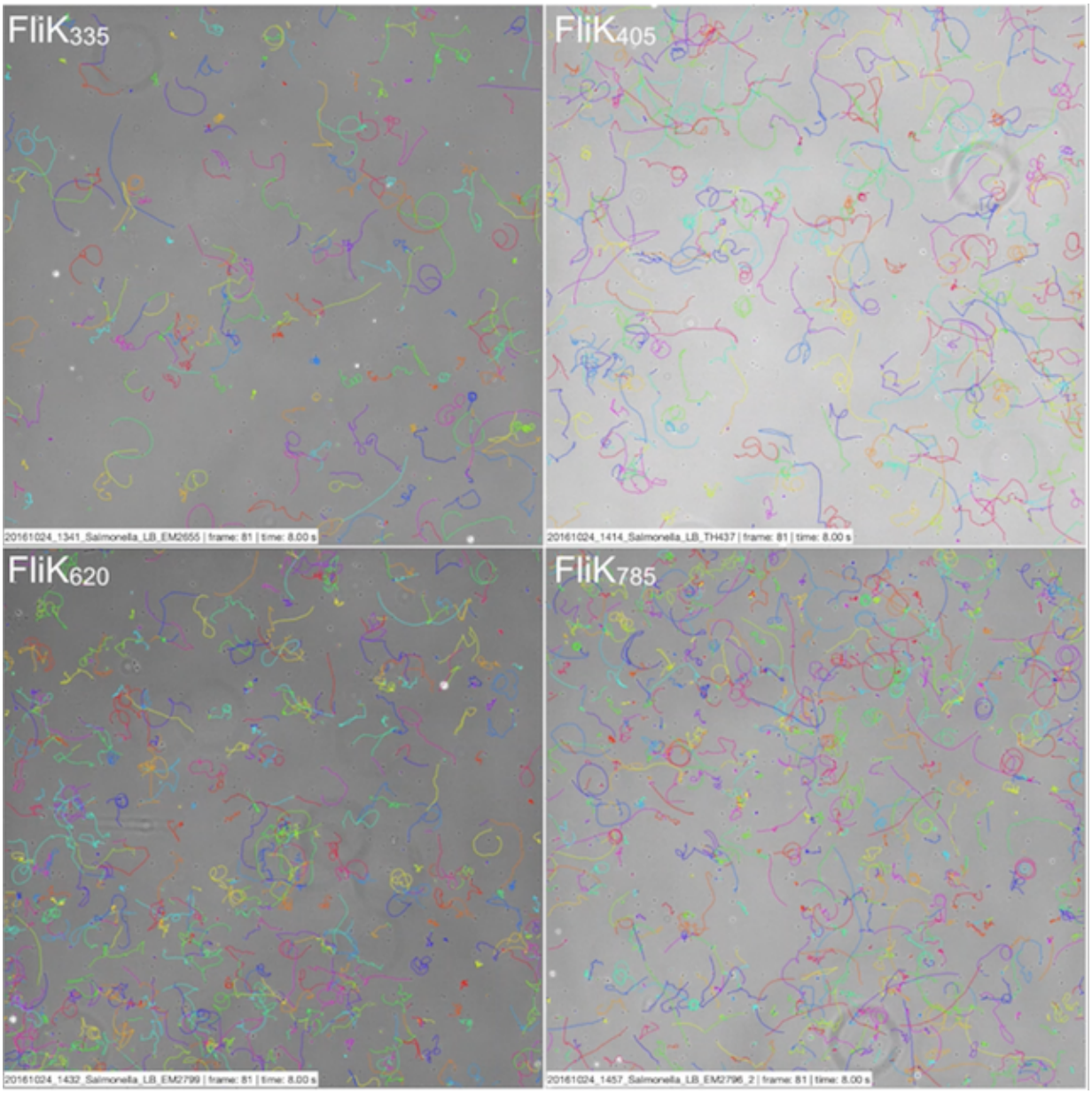

Supplementary Movie S1: Motility performance of hook length variants revealed by single-cell tracking in quasi 2D. Exemplary movies illustrating the swimming behavior of FliK335, FliK405 (wt), FliK620 and FliK785 are shown.